**Progress in Oceanography**
January 2023, Volume 210 Pages 102949 (18p.)
https://doi.org/10.1016/j.pocean.2022.102949
https://archimer.ifremer.fr/doc/00813/92490/



# Hydrology and small pelagic fish drive the spatio–temporal dynamics of springtime zooplankton assemblages over the Bay of Biscay continental shelf

Grandremy Nina [1, *], Romagnan Jean-Baptiste [1, *], Dupuy Christine [2], Doray Mathieu [1], Huret Martin [3], Petitgas Pierre [4]

[1] DECOD (Ecosystem Dynamics and Sustainability), IFREMER, INRAE, Institut Agro, Nantes, Centre Atlantique - Rue de l'Ile d'Yeu - BP 21105, 44311 Nantes Cedex 03, France
[2] BIOFEEL, UMRi LIENSs, La Rochelle Université / CNRS, France
[3] DECOD (Ecosystem Dynamics and Sustainability), IFREMER, INRAE, Institut Agro, Brest, France
[4] IFREMER, RBE, Centre Atlantique, 44311 Nantes Cedex 03, France

* Corresponding author : Nina Grandremy, email address : grandremy.n@gmail.com ; Jean-Baptiste Romagnan, email address : jean.baptiste.romagnan@ifremer.fr

cdupuy@univ-lr.fr ; mathieu.doray@ifremer.fr ; martin.huret@ifremer.fr

**Abstract :**

As mesozooplankton is the preferential prey of small pelagic fish (SPF), environmentally–driven mesozooplankton dynamics can have critical effects on SPF population dynamics. Despite previous studies on SPF habitats' dynamics, hydrological landscapes and mesozooplankton dynamics in the Bay of Biscay (BoB), knowledge gaps persist at the BoB regional–scale pelagic ecology and in particular about the mesozooplankton assemblages and their long–term space–time patterns. Here, we present 16 years of spring mesozooplankton assemblage interannual spatial dynamics over the BoB continental shelf and we describe the correlations between the mesozooplankton space–time patterns and those in hydrology, primary producers and SPF. We gathered data originating from the PELGAS surveys (2004–2019) and remote sensing products. Mesozooplankton samples were collected with a 200–µm mesh size WP2 net vertically towed from 100 m depth (or 5 m above the sea floor) to the surface. They were analysed with imaging and deep-learning tools and the biomass in 24 coarse taxonomic groups was calculated. Automated procedures for spatial gridding and missing data imputation enable the generation of yearly maps time series with the same spatial resolution across the pelagic ecosystem components and years. These comprehensive multivariate datasets were analysed with a multi–table method known as Multiple Factor Analyses to depict time–consistent spatial patterns in each ecosystem component and the temporal variability around them. Finally, the main time–consistent spatial patterns in the hydrology, primary producers and SPF ecosystem components were used as predictors in generalized linear models, to explain those in the mesozooplankton. Mesoscale coastal-offshore and north–south gradients were the main patterns observed in each of the pelagic ecosystem components studied. The spatial patterns in the mesozooplankton assemblage were stable, without any significant changes detected in the taxonomic composition nor its spatial structure over the studied period. Small copepods, gelatinous and meroplanktonic organisms characterised coastal areas. Euchaetidae and meroplanktonic crustaceans' larvae displayed higher biomass in the northern part of the BoB while Metridinidae, Cladocera,

Appendicularia and Echinodermata had higher biomass in the southern part. Surface and bottom water temperature, salinity–related parameters, water column stratification and SPF biomasses were the variables that best explained the observed space–time patterns in the mesozooplankton communities.

**Highlights**

► Taxonomically and spatially–resolved zooplankton dataset over 16 years in spring. ► Time–consistent zooplankton composition spatial structure with multi–table analysis. ► Explanation of zooplankton spatial patterns with gradients in the pelagic ecosystem. ► Zooplankton spatial pattern underpinned by taxonomic composition and size structure. ► River plumes, temperature gradients and pelagic fish correlated zooplankton pattern.

**Keywords** : Mesozooplankton, Imaging analysis, Time–consistent spatial patterns, Ecosystem structure, Spring habitat, Multi Factor Analysis, Bay of Biscay

# 1 Introduction

Mesozooplankton is the preferential prey of small pelagic fish (SPF, e.g. sardine and anchovy; Plounevez and Champalbert, 1999; Van Der Lingen, 2002; Bachiller and Irigoien, 2015; Fonseca et al., 2022). It is therefore a key trophic link that enables the transfer of matter and energy from the primary production to higher trophic levels in oceanic (Banse, 1995), upwelling ecosystems (Rykaczewski and Checkley, 2008) as well as in continental shelf ecosystems (Irigoien et al., 2008; Dessier et al., 2018; Noyon et al., 2022).

The short generation time of mesozooplankton and their sometimes non-linear response to environmental changes make them sensitive to environmental variability from small spatio-temporal scales (*i.e.* Romagnan et al., 2015, 2016) to long term, global scale climate change (Hays et al., 2005; Batchelder et al., 2012; González-Gil et al., 2015). Yet, the diversity of taxa, morphologies and size ranges often make difficult to sample, analyse and model this important ecosystem component at the appropriate spatio-temporal as well as biological resolutions (Mitra and Davis, 2010). Further, the diversity of mesozooplanktonic organisms' life cycles and habitat requirements translate into a variety of community dynamics that may require local to large scales, and populations to communities' studies for their understanding.

Numerous studies suggest a potentially critical effect of environmentally driven mesozooplankton dynamics on SPF population dynamics in various ecosystems worldwide (*i.e.* Cury et al., 2000; Van Der Lingen, 2002; Rykaczewski and Checkley, 2008; Capuzzo et al., 2018). In the European waters, recent studies highlighted the probable bottom-up effects of mesozooplankton-mediated decline in SPF body condition and size in the Gulf of Lion (NW Mediterranean, Saraux et al., 2019). The authors hypothesized that a decadal shift towards smaller mesozooplanktonic species in the Mediterranean adversely affected the potential energy income of SPF (Queiros et al., 2019 but see Feuilloley et al., 2022). A similar decadal trend in the decline in SPF size at age has recently been evidenced over the 2000-2015 period (Doray et al., 2018b), throughout the French continental shelf of the Bay of Biscay (hereafter BoB), an open ocean bay delimited by the Spanish coast (south) and the French coast (east & north). However, a comprehensive explanatory study still needs to be set up. This study is a first step towards this goal, and aims at understanding the mesozooplankton

habitat distribution, and its correlations with variables describing the pelagic ecosystem components, from hydrology (water temperature, salinity, water column stratification index) to higher trophic levels (SPF).

A corpus of data and studies on the SPF habitats' patterns and dynamics exists in the BoB (Petitgas et al., 2018; Doray et al., 2018c, 2022), as well as for hydrological landscapes (Koutsikopoulos et al., 1998; Castaing et al., 1999; Planque et al., 2004; Guillaud et al., 2008). Distribution patterns of mesozooplankton have also been described but in the south-eastern area of the BoB only (Albaina and Irigoien, 2007a; Dessier et al., 2018) and in the adjacent Cantabrian shelf (Albaina and Irigoien, 2007b; Iriarte et al., 2022). Coastal waters show larger biomass and smaller organisms than offshore waters (Sourisseau and Carlotti, 2006; Vandromme et al., 2014), and are dominated by copepods and meroplanktonic organisms (Irigoien et al., 2008; Dessier et al., 2018). Mesoscale oceanographic structures *i.e.* river plumes and shelf-break fronts (Albaina and Irigoien, 2004, 2007b), hydrological features (*i.e.* water column stratification), winter mixing and microphytoplankton abundance were identified as drivers of mesozooplankton dynamics (González-Gil et al., 2015; Dessier et al., 2018). Nevertheless, important knowledge gaps persist at the scale of the BoB and small pelagic fish populations, as the spatial coverage of existing mesozooplankton studies was consistently focused on the south of the BoB (South of 46°30N) although the North is ecologically important *e.g.* as SPF spawning, feeding and nursery habitats (Bellier et al., 2007; ICES, 2010). In addition, currently available mesozooplankton space-time data series are often short: the longest spatially resolved series spans from 2003 to 2013 (Dessier et al., 2018), making the detection of long term changes detected in many other ecological components (Chust et al., 2022) more difficult for the mesozooplankton. Therefore, important uncertainties remain about the patterns of mesozooplankton assemblages and their long-term space-time evolution, at the scale of the entire BoB, in the context of accelerating ecological changes due to the local effects of global warming (Chust et al., 2022).

Here, we present the first comprehensive space-time analysis of the mesozooplankton community over 16 years (2004 to 2019), in spring, over the BoB continental shelf. The spatial coverage of our study spans from the coast to the shelf break, and from the eastern Spanish coast to southern Brittany coastal waters, therefore encompassing the whole French BoB continental shelf (Fig. 1).

Mesozooplankton samples collected during the pelagic ecosystem survey PELGAS (Doray et al., 2018c) were analysed with imaging tools (Gorsky et al., 2010; Colas et al., 2018) to achieve a coarse but consistent taxonomic resolution throughout the series. The homogeneity and completeness in the data spatial resolution over time was guaranteed using a gridding smoothing procedure (Masse et al., 2018 section 3) and a missing data imputation technique (Josse and Husson, 2016) when necessary. The same data preparation procedure was applied to concomitant hydrology, primary producers and SPF data series originating from the PELGAS surveys and remote sensing data to generate a comprehensive dataset with the same space-time resolution across the pelagic ecosystem components. Our goal is to explore the variability in the spatial patterns over time in the BoB mesozooplankton assemblage and how they correlate with the other pelagic ecosystem components. The mesozooplankton component was studied here considering its estimated biomass to produce time series of maps that could be integrated in future zooplankton modelling studies. This new data could be integrated to marine food web studies, which are often based on biomass data. This spatial ecology approach is a first step in identifying potential bottom-up and top-down controls exerted on the BoB mesozooplankton assemblage, in a climate change context.

# 2 Materials and methods

## 2.1 The PELGAS survey

The PELGAS integrated survey takes place every year in spring since 2000, over the French continental shelf of the BoB. The aim of this survey is to assess small pelagic fish biomass and monitor the pelagic ecosystem, to inform ecosystem based fisheries management. Concomitantly with fish data, hydrology, phyto- and zoo-plankton samples and megafauna sightings (marine mammals and seabirds) are collected to build long-term spatially-resolved time series of the BoB pelagic ecosystem. The PELGAS sampling strategy combines en-route data collection (small pelagic fish and megafauna) during the day, with fixed points, depth-integrated hydrology and plankton sampling during the night (Fig. 1). Detailed PELGAS survey protocols can be found in Doray et al., 2018b and 2021.

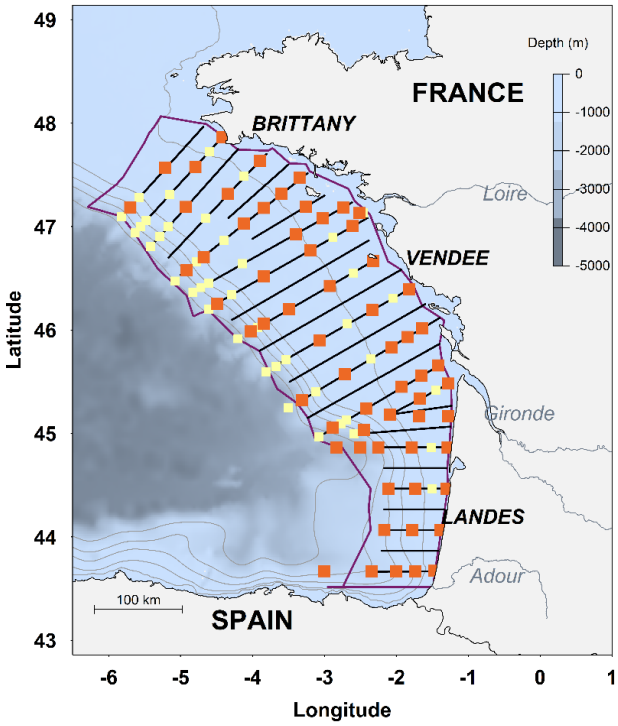


Fig. 1: PELGAS sampling scheme. Solid black lines: acoustic prospection transects for the evaluation of SPF biomass. Squares: Fixed-point water column sampling for hydrology parameters (light yellow) or hydrology parameters and plankton (orange) sampling. Note that the fixed-point geographical positions and sampling may change from year to year. Solid purple line: area considered for this study. Light grey lines: 100 to 500 m isobaths.

## 2.2 Mesozooplankton samples collection

Mesozooplankton samples were collected with vertical hauls of 200-µm mesh size WP2 net, from 100 m depth (or 5 m above the sea floor) to the surface. In 2004 and 2005, the sampling maximum depth was 200 m. Since 2014, the net has been equipped with a flowmeter (Hydrobios) to measure the sampled water volume. Before 2014, the sampled water volume was estimated by multiplying the deployed cable length by the net opening surface (0.25 $m^2$). From 2004 to 2019, the number of sampling points varied between 41 and 64 per year, due to adjustments in the sampling strategy and weather conditions. Between 2004 and 2016, 699 samples were collected and preserved in 4% formaldehyde on board for further analysis back on land. Between 2017 and 2019, 190 samples were collected and were analysed live on board. Both sets of samples were analysed with imaging instruments.

## 2.3 Mesozooplankton analyses and data

The preserved samples (2004-2016) were digitized on land with the ZooScan, a waterproof flatbed scanner generating 16 bit gray-level high resolution images (pixel size: 10.56 µm, 2400 dpi) (Gorsky et al., 2010). Prior to digitization, the samples were size-fractionated with a 1 mm sieve, into organisms > 1 mm and <1 mm size fractions, to avoid underestimation of large and rare objects due to subsequent subsampling. Then, both fractions were separately subsampled with a Motoda splitter, to obtain sub-samples containing 500-1500 objects. Each subsample was imaged after manual separation of objects on the scanning tray, to minimize the occurrence of touching objects (Vandromme et al., 2012). Remaining touching objects were manually digitally separated with a custom Zooprocess tool to ensure the quality of further identifications and counts. From 2017 onwards, the samples were analysed live on board with the ZooCAM, an in-flow imaging instrument (pixel size: 10.3 µm) allowing the quasi real time analysis of samples (Colas et al., 2018). Samples were split as a single fraction with a Motoda splitter before being digitized. The agreement between the ZooScan and the ZooCAM in identifying similar communities and producing similar total mesozooplankton abundances and size distributions was demonstrated earlier (Colas et al., 2018). All raw images generated with both instruments were processed to obtain individual vignettes of each object digitized and associated morphological features,

including the size in pixels of each object. All individual planktonic vignettes were classified using Ecotaxa (Picheral et al., 2017), a dedicated online tool that combines a Random-Forest and a Convolutional Neural Network to achieve automatic identification, which is now a classic semi-automatic identification procedure. Each identified object, originating from both instruments, was then visually checked and explicitly validated or corrected when necessary, using Ecotaxa again. Eventually, 2,135,401 objects were analysed and sorted into 24 broad taxonomic groups, to achieve a trade-off between the diversity of the taxa seen in the area, and the identification skills of experts who validated the automatic classification results. The taxonomic resolution is detailed in Table 1. Some taxonomic groups aggregate a diversity of species. For example, the group “Eumalacostraca” comprised adult forms of crustaceans such as Amphipods, Decapods and Isopods. The group “Meroplankton crustacean larvae” consisted of larval forms of meroplanktonic crustaceans, for example Cirripedia, Brachyours and Decapods zoe. The category “Crustacean nauplii” grouped the nauplii forms of holoplanktonic crustaceans, mostly copepods (Table 1). Non-living objects (i.e. detrituses, large aggregates, artefacts) and remaining multiple objects were excluded from the dataset.

Then, the biomass expressed in µg Dry Weight of each object was calculated from each object’s individual surface in pixels converted to $mm^2$, following Lehette and Hernández-León (2009) and Garijo and Hernández-León (2015) (Table 1). These equations are a common way to estimate biomasses of coarse zooplankton taxa and were used in zooplankton studies in the Southern Ocean (Stirnimann et al., 2021; Kerkar et al., 2022), tropical oceans and temperate environments (Marcolin et al., 2015; Garcia-Herrera et al., 2022; Giering et al., 2019; Makhlouf Belkahia et al., 2021; Noyon et al., 2022) and at the global scale (Hernández-León et al., 2020; Soviadan et al., 2022), in open ocean as well as in shelf seas. The biomass of each taxonomic group was calculated at every sampling station, by summing the objects’ biomass within each taxonomic group, multiplied by the subsampling ratio and divided by the sampled water volume, to obtain the biomass expressed in µg Dry Weight.$m^{-3}$ for each taxa, at each sampling point. The organisms’ size considered in this study ranged between 0.3 and 3.4 mm ESD (large mesozooplankton). Data from both instruments were finally assembled to form a spatially-resolved dataset comprising 24 mesozooplankton taxa over 16 years from 2004 to 2019.

Table 1: Mesozooplankton taxonomic groups used to characterise mesozooplankton spring community in the Bay of Biscay; the conversion equations of body area "A" ($mm^2$) into dry weight (µg Dry Weight) were found in Lehette & Hernandez – Leon (2009) and Garijo & Hernandez – Leon (2015).

| Organisms | Taxonomic groups | Code | Dry weight |
|---|---|---|---|
| Copepods | Acartiidae | Acart | $43.97 * A^{1.52}$ |
| | Calanidae | Cal | |
| | Centropagidae | Centrop | |
| | Euchaetidae | Euch | |
| | Metridinidae | Metri | |
| | Temoridae | Temo | |
| | Other Calanoida | Calano | |
| | Cyclopoida | Cyclo | |
| | Harpacticoida | Harpact | |
| | Poecilostomatoida | Poecil | |
| Other crustaceans | Eumalacostraca | Eumal | |
| | Meroplankton crustacean larvae | Larv_mero | |
| | Crustacean nauplii | Npl_crust | |
| | Cladocera | Clad | |
| General euphausiids | Shrimp-like | Shrimp | $49.58 * A^{1.48}$ |
| Chaetognaths | Chaetognaths | Chaeto | $23.45 * A^{1.19}$ |
| Cnidarian: Siphonophores | Siphonophores | Sipho | $43.17 * A^{1.02}$ |
| Other gelatinous plankton | Appendicularians | Append | $4.03 * A^{1.24}$ |
| | Thaliacea | Thal | |
| | Other Cnidarians | Cnid | |
| Other plankton | Bivalvia larvae | Biv | $43.38 * A^{1.54}$ |
| | Fish larvae | Actin | |
| | Echinodermata larvae | Echin | |
| | Thecosomata | Thec | |

237

## 2.4 Hydrology and primary producers data

At-station vertical profiles were performed with a conductivity-temperature-depth (CTD, SeaBird SBE19 + V2) probe fitted with a fluorimeter and Niskin bottles, to conduct hydrological and phytoplankton sampling. Several water column structure descriptors were calculated from CTD casts, at each sampling station (Table 2): the surface salinity (mean between 2 and 7 m), the bottom temperature (value recorded at 5 m above the seabed), the equivalent freshwater height, and three water column stratification indices: the potential energy deficit, the mixed layer maximum depth, and the pycnocline depth. The equivalent freshwater height is an index of river plume influence, which measures the freshwater height over the water column, considering a salinity reference value set at 35.5 psu. It better integrates the recent history and local influence of river run-offs and is less sensitive to vertical mixing than surface salinity. The deficit of potential energy is an index of water column stratification, defined as the energy necessary to homogenise the water density over the water column. A detailed description of these water column descriptors can be found in Huret et al. (2013).

Water samples collected with the Niskin bottles at the surface were filtered on board, stored at -80°C and further analysed by spectrophotometry back on land, to estimate the total and size-fractionated chlorophyll-*a* concentration (pico- (< 3 µm), nano- (3-20 µm) and micro-phytoplankton (> 20 µm)). The water column integrated chlorophyll-*a* concentration was estimated using the fluorescence data from the vertical profiles which was calibrated with the actual measures of chlorophyll-*a* concentrations at three depths (surface, deep chlorophyll maximum, and below the thermocline).

Sea surface temperatures (SST) and surface chlorophyll-*a* concentrations from remote sensing data were downloaded from https://marine.copernicus.eu/ (named as SST_ATL_SST_L4_REP_OBSERVATIONS_010_026 and OCEANCOLOUR_ATL_CHL_L4_REP_OBSERVATIONS_009_098, respectively). The downloaded SST data products were derived from AVHRR sensors of NOAA satellites daily products, and interpolated to fill in missing data due to the clouds, following Saulquin and Gohin (2010). Surface chlorophyll-*a* concentration data were derived from several sensors (SeaWiFS, MERIS, MODIS) and processed following Gohin (2011).

Table 2: Parameters used to describe the hydrological conditions and the primary producers structure in the Bay of Biscay, in spring.

| Ecosystem component | Parameter | | Code | Units | Time series | Source |
|---|---|---|---|---|---|---|
| Hydrology | Bottom temperature | | BTemp | °C | 2004 - 2019 | PELGAS surveys |
| | Potential energy deficit | | PotEDef | $Kg.m^{-1}.m^{-2}$ | | |
| | Equivalent freshwater height | | EqFH | meters | | |
| | Mixed layer depth | | MLD | | | |
| | Pycnocline depth | | PycnD | | | |
| | Surface salinity | | SSal | psu | | |
| | Surface temperature | | STemp | °C | | Satellite data |
| Primary producers | Size-fractionated surface chlorophyll-*a* concentration | < 3 µm | Chl3 | $mg.m^{-3}$ | 2009 - 2019 | PELGAS surveys |
| | | 3 - 20 µm | Chl-3-20 | | | |
| | | > 20 µm | Chl20 | | | |
| | Total surface chlorophyll-*a* concentration | | TotChl | | | |
| | Integrated chlorophyll-*a* | | IntChl | $mg.m^{-2}$ | | |
| | Chlorophyll-*a* maximum concentration depth | | ChlMD | meters | | |
| | Chlorophyll-*a* concentration | | satChl | $mg.m^{-2}$ | | Satellite data |

## 2.5 Small pelagic fish biomass

Small pelagic fish acoustic densities were recorded at 10 knots during daytime, along transects using a calibrated monobeam echosounder operating at 38 kHz. Midwater trawl hauls were adaptively performed to identify to species the echotraces and provide their length, weight and age composition. Acoustic and biotic trawl data were combined using the standard methodology described in Doray et al. (2021) to derive biomass estimates per species and 5 cm length classes, within one nautical mile (1852 m) long Elementary Sampling Units along the survey track. Biomass estimates were expressed in tonnes per nautical miles square ($tonnes.nm^{-2}$). The SPF species appearing in at least 50 % of the 16 PELGAS surveys considered (2004-2019) were selected to characterise the fish component. Selected species included boarfish (*Capros aper*), Atlantic chub mackerel (*Scomber colias*), Atlantic mackerel (*Scomber*

283 *scombrus*), Atlantic horse mackerel (*Trachurus trachurus*), Mediterranean horse
284 mackerel (*Trachurus mediterraneus*), blue whiting (*Micromesistius poutassou*),
285 European anchovy (*Engraulis encrasicolus*), European sardine (*Sardina pilchardus*)
286 and sprat (*Sprattus sprattus*) (Table 3).

Table 3: Time series of small pelagic fish species considered by 5 cm length classes.

| SPF species | Code | Length class | Time series (n years) |
|---|---|---|---|
| Boarfish (*Capros aper*) | CAPR-APE | (10, 15] | 2004 - 2019 (9) |
| European anchovy (Engraulis encrasicolus) | ENGR-ENC | (5, 10] | 2006 - 2019 (8) |
| | | (10, 15] | 2004 - 2019 (16) |
| | | (15, 20] | |
| Blue whiting (Micromesistius poutassou) | MICR-POU | (15, 20] | 2004 - 2017 (11) |
| | | (20, 25] | 2004 - 2019 (15) |
| | | (25, 30] | 2005 - 2019 (14) |
| European sardine (Sardina pilchardus) | SARD_PIL | (10, 15] | 2005 - 2019 (13) |
| | | (15, 20] | 2004 - 2019 (16) |
| | | (20, 25] | |
| Atlantic chub mackerel (*Scomber colias*) | SCOM-COL | (15, 20] | 2004 - 2018 (14) |
| | | (20, 25] | 2004 - 2019 (16) |
| | | (25, 30] | 2004 - 2019 (15) |
| | | (30, 35] | 2004 - 2019 (14) |
| | | (35, 40] | 2005 - 2019 (9) |
| Atlantic mackerel (Scomber scombrus) | SCOM-SCO | (15, 20] | 2005 - 2019 (11) |
| | | (20, 25] | 2004 - 2019 (16) |
| | | (25, 30] | |
| | | (30, 35] | |
| | | (35, 40] | |
| European sprat (Sprattus sprattus) | SPRA-SPR | (5, 10] | 2004 - 2019 (13) |
| | | (10, 15] | 2004 - 2019 (16) |
| Atlantic horse mackerel (*Trachurus trachurus*) | TRAC-TRU | (10, 15] | 2004 - 2019 (16) |
| | | (15, 20] | |
| | | (20, 25] | |
| | | (25, 30] | |
| | | (30, 35] | 2004 - 2019 (13) |
| Mediterranean horse mackerel (Trachurus mediterraneus) | TRAC_MED | (15, 20] | 2005 - 2018 (10) |
| | | (20, 25] | 2006 - 2019 (10) |
| | | (40, 45] | 2006 - 2019 (9) |

287 A summary of the data used in this study can be found in Fig. 2 (top panel).

## 2.6 Data gridding and missing data imputation

Although the biological and physico-chemical sampling are rather regular and homogeneous on the PELGAS cruise (Doray et al., 2018c), the spatial resolution and number of samples may vary across years and between variables. Therefore, a block averaging procedure (Petitgas et al., 2009, 2014) was consistently applied on each of the datasets before conducting any further analysis. All variable used were gridded over a common spatial grid. The grid mesh size was set at 0.3° in both latitude and longitude, a compromise between the grid mesh size commonly set at 0.25° in previous studies based on spatially resolved datasets (Doray et al., 2018a; Masse et al., 2018; Petitgas et al., 2018) and the distance between the mesozooplankton sampling stations, to limit the number of grid cells without data. The grid origin x0 was initially positioned at 43°N and 6°W and then drawn randomly within a two cells radius, 300 times. Data were averaged in each grid cell for every origin position, in order to minimize the influence of the origin position on gridded values. Finally, 300 mean values were averaged to calculate a spatially smoothed estimate in each grid cell (Fig. 2, step 1). Grid cells having their center point inside the polygon defining the survey area were kept for the analysis (n = 121) (Fig. 1). The block averaging step was realized with the EchoR *R* library (Doray et al., 2013).

After the block averaging step, some cells were still empty (missing data). These missing data are the consequence of missing sampling stations, especially in the northern part of the BoB, mostly at the beginning of the time series (Appendix A, Table A.1). To fill data gaps in particular grid cells and years, we applied a missing data imputation procedure (Josse and Husson, 2016). Each variable was organized into matrix form, grid cells x years. An algorithm based on iterative Principal Component Analysis (PCA) was applied to each data matrix, to impute predicted data point values to the empty cells (Fig. 2, step 2). The iterations were run until the difference between two successive estimated values was smaller than a threshold (set at 1e-06). Sometimes, the final predicted values were negative. In this case, we imputed the mean of the adjacent grid cells to the empty cell. A comparison of annual spatial patterns and annual means, calculated with and without the imputed values, was used as a quality check of the imputed values. This missing data imputation method was implemented using the MissMDA *R* library (Josse and Husson, 2016).

Eventually, the complete dataset is composed of sets of gridmaps for parameters in the hydrology, primary producers, mesozooplankton and SPF components. All the gridmaps have the same spatial extent and resolution and span from 2004 to 2019, except for primary producers dataset which span from 2009 to 2019.

## 2.7 Data analysis

All the data analyses were performed using the *R* statistical language version 4.0.3 (R Core Team, 2020). The analytic pipeline is organized as follow. First, we applied a Multiple Factor Analysis (MFA, see below for details) on each ecosystem component (Fig. 2, step 3). Then the mesozooplankton MFA results were used to input a hierarchical clustering (Fig. 2, step 4). Finally, results from the hydrology, primary producers and fish MFA were used as explanatory variables in Generalized Linear Models (GLMs) to explain the observed mesozooplankton space-time patterns (Fig. 2, step 5).

### *2.7.1 Multiple Factor Analysis*

Multiple Factor Analysis (MFA, Escofier and Pagès, 1994; Pagès, 2014) has recently been applied to characterise space-time patterns in series of multivariate gridmaps of ecological variables (Abdi et al., 2013; Doray et al., 2018a; Petitgas et al., 2018). MFA is a multi-table statistical method based on PCA and designed to analyse 3D structured datasets, in which the variables are organized in tables of the same size, over time. Here, the grid cells correspond to the tables' rows (1$^{st}$ dimension: *n* individuals), the variables the columns (2$^{nd}$ dimension: *m* variables), and the tables are stacked (3$^{rd}$ dimension: *p* groups), to obtain a multivariate time series of yearly tables. It is worth noticing that MFA applies even when the number of available variables differ over time.

Similarly as with PCA and a 2D dataset, MFA results in summarizing a 3D dataset into a factorial space, in which all individuals (*i.e.* grid cells), variables and tables (years) can be represented (Pagès, 2014). Eventually, each grid cell can be located in each year in the factorial space around its (time) average position and similarly for each variable. MFA enables the estimation of a common multivariate correlation structure over all years, and its associated time variability. The individuals being grid cells here, the target structure is a spatial pattern with its time variability. For a detailed

description of MFA implementation, see Petitgas et al., 2018, § 3.3 - 3.5, pp 191-193, and Doray et al., 2018 § 2.5-2.7, p 91.

### *2.7.2 MFA implementation and principal components selection*

Specific MFAs were applied separately on the hydrology, primary producers, mesozooplankton and SPF datasets, to characterize their space-time patterns. Data from biotic components (primary producers, mesozooplankton and SPF) were log-transformed to reduce the skewness in their distributions. Hydrology and primary producers variables were centred and normalized in each year to account for the differences in units and ranges. Mesozooplankton and SPF variables were centred only (all variables in these two datasets have the same units), thus leaving the differences in variance between years affect time variability. The MFAs were implemented using the function *MFA* from the FactoMineR *R* library (Lê et al., 2008).

Similarly to a classic PCA, MFA can be used to reduce the dimensionality, filter and synthetize complex datasets by selecting only a few first principal components (*PCs*) for subsequent analyses. When using MFA on time resolved datasets, it is important to consider not only the percentage of total variance explained by the MFA *PCs* (Fig. 4), but also the number of significant correlations between each *PC* and the years (*i.e.* tables) to assess the representativity of each *PC* over time (Pagès, 2014). We selected the *PC*s that showed correlations with the years higher than a threshold for at least half of the total number of years. Such threshold was estimated following Pagès (2014), using the maximum value of correlation between years and high orders *PCs*, here *PC.4* and *PC.5* (see the results of this procedure in Fig. 5).

Then, each selected *PC* was interpreted considering its correlation with the variables. The variables retained to interpret the *PCs* showed a correlation coefficient greater than |0.5| with the *PCs* for at least half of the total number of years. Further, mean individuals' (grid cells') coordinates on the *PCs* were mapped at their geographical positions. The MFA selected *PCs* were used as synthetic descriptors for each of the ecosystem component datasets.

### *2.7.3 Mesozooplankton space-time patterns: hierarchical clustering*

The average spatial structure of the mesozooplankton community was identified by applying a Hierarchical Agglomerative Clustering (function *hclust* in *R* language,

Ward's method, Euclidean distance, without spatial constrain) on the mean individuals' (grid cells') coordinates in the mesozooplankton MFA factorial space. The function NbClust from the R library NbClust (Charrad et al., 2014) was used to determine the optimal number of clusters through the calculation of thirty partitioning indices. The best number of clusters is defined as the one suggested by the highest number of indices. Then, grid cell clusters were mapped, to characterise regions with time-consistent specific mesozooplankton assemblages. The taxonomic composition of each cluster was assessed by calculating the annual mean of the variables (taxa) in each cluster. Only the taxa showing a correlation coefficient greater than |0.5| with the mesozooplankton MFA *PCs* for at least half of the total number of years were considered. Variables being centered, the annual mean biomass of a taxa within a cluster represents its residual variation relative to the global mean taxon biomass over all the grid cells and years. Finally, each grid cell in each year was associated to the nearest cluster centroid in the MFA space to estimate the annual spatial distribution of the clusters and to characterize the interannual variability in the clusters. The frequency of grid cells affiliation within each cluster was also calculated over the time series, and mapped.

### *2.7.4 Correlates of the observed mesozooplankton space-time patterns*

The MFA *PCs* for the hydrology, primary producers and SPF ecosystem components (referred to as predictors hereafter) were used as explanatory variables in GLMs, where the MFA *PCs* for the mesozooplankton were the dependent variables. For each *PC* selected in the mesozooplankton MFA, we first built a model using all the predictors. We checked for collinearity in the predictors by using the Variance Inflation Factor (VIF, Fox and Monette, 1992). A VIF value higher than five was used to identify problematic multicollinearity among predictors. VIF was calculated using the car *R* library (Fox and Weisberg, 2019). Predictors explaining less variance and displaying high multicollinearity (VIF criterion) were removed. Then, a stepwise backward model selection procedure was applied (function *stepAIC* in *R* language) to select the most significant predictors based on Akaike's Information Criterion (AIC) (Burnham et al., 2002). Models were considered significantly different when their AIC difference was higher than two. Finally, an ANOVA was used on the model selected to rank the predictors by their explicative power.

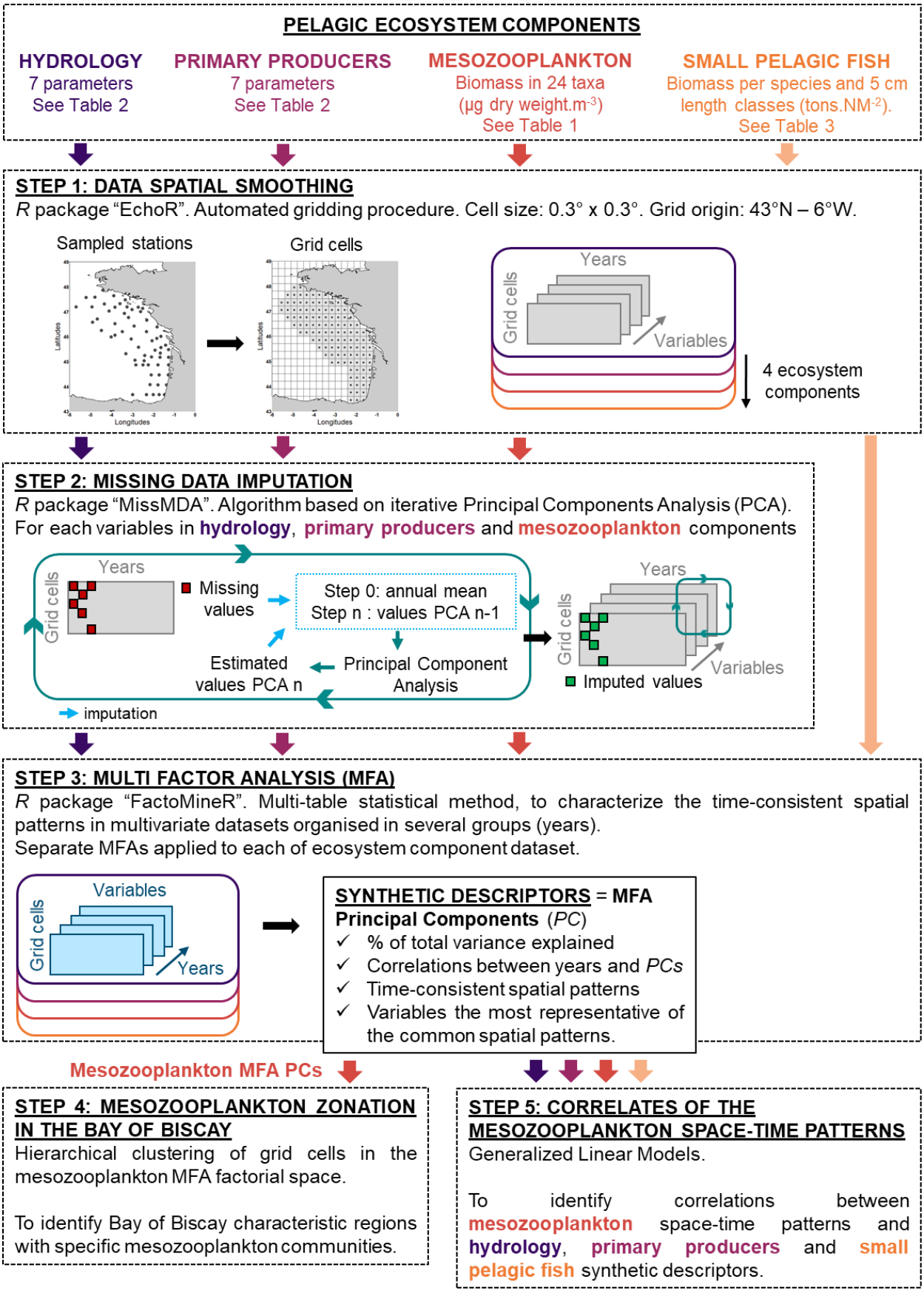


Fig. 2: Summary of the steps followed for the datasets construction and analysis.

# 3 Results

## 3.1 Taxonomic composition and total biomass of the mesozooplankton community

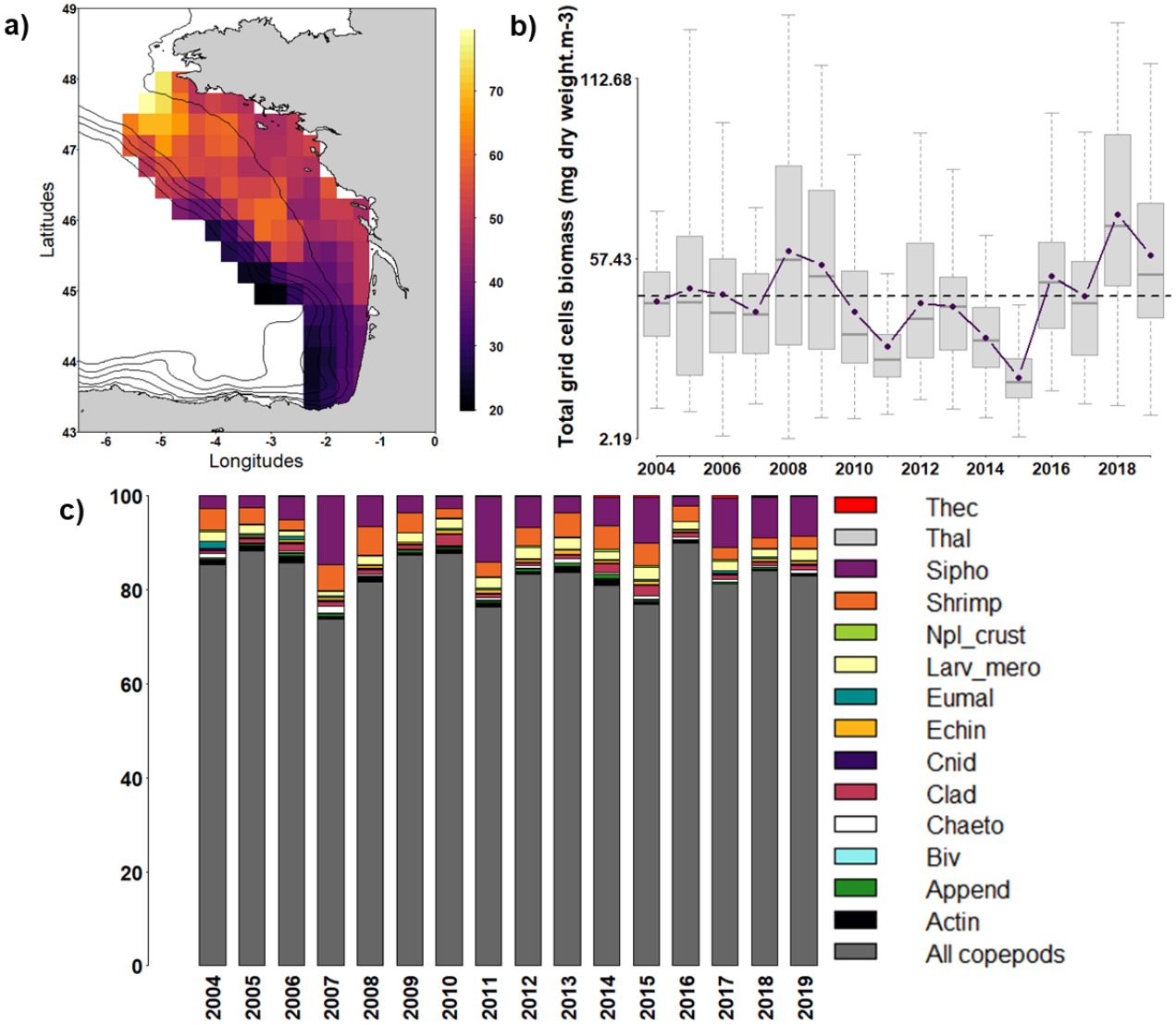


Fig. 3: (a) Mesozooplankton community total biomass (mg dry weight.m$^{-3}$) mean map, averaged between 2004 and 2019. (b) Grid cells total biomass yearly distributions from 2004 to 2019. Boxplots: total biomass by grid cells (n = 121). The dashed line is the mean total biomass over the time series. Solid line: annual means. (c) Taxonomic groups relative contributions to the mesozooplankton community total biomass (percentage). The ten copepod groups were summed and plotted as one group for more clarity.

The mean map of total biomass per grid cell, from 2004 to 2019, revealed a North-South gradient. Highest total biomass was observed north to 45.5°N between the 100 m and 200 m isobaths, where the biomass ranged between 60 and 80 mg dry weight.$m^{-3}$, whereas the lowest values ranged between 20 and 30 mg dry weight.$m^{-3}$ south of 45.5°N, on the continental shelf slope (Fig. 3a). Total biomass yearly distributions did not show a clear temporal trend, but the lowest values occurred from 2010 to 2015. The lowest annual means occurred in 2011 and 2015 (30.5 ± 16 mg dry weight.$m^{-3}$ and 21 ± 8.6 mg dry weight.$m^{-3}$, respectively), while the highest ones occurred in 2008 and 2018 (59.8 ± 33.3 mg dry weight.$m^{-3}$ and 71 ± 30.5 mg dry weight.$m^{-3}$, respectively) (Fig. 3b). The copepods dominated the mesozooplankton community every year, contributing from 73% (2007) to 90% (2016) to the community total biomass. Siphonophores was the second most important taxonomic group, representing up to 14% of the total biomass in 2007 and 2011. These two groups had opposite trends in their contributions, the years of minimum contribution of one corresponding to the years of the maximum contribution of the other (Fig. 3c).

## 3.2 MFA *PCs* selection for each ecosystem component.

The first three *PCs* of the hydrology MFA (referred to as hydroMFA1, hydroMFA2 and hydroMFA3 hereafter) explained 72.8 % of the space-time variance in the hydrology dataset (Fig. 4). In this case, the correlation threshold for retaining MFA *PCs* as meaningful was set to 0.73 (see Methods section 2.7.2). All the years of the hydrology time series showed correlations higher than 0.73 to the hydroMFA1 (n = 16) and the hydroMFA2, except 2007 (hydroMFA2, n = 15). Ten years were correlated with a coefficient > 0.73 to hydroMFA3 (Fig. 5a). The first *PC* of the primary producers MFA (referred to as phytoMFA1 hereafter) explained 36.7 % of the space-time total variance in the primary producers dataset (Fig. 4). It was the only *PC* showing correlation coefficients with years (n = 11) higher than the threshold (here set to 0.67, see Methods section 2.7.2) (Fig. 5b). The first two *PCs* of the mesozooplankton MFA (referred to as zooMFA1 and zooMFA2 hereafter) explained 50.5 % of the space-time variance in the mesozooplankton dataset (Fig. 4). All the years (n = 16) of the mesozooplankton time series were correlated to the zooMFA1 with a coefficient higher than the threshold (here set to 0.83, see Methods section 2.7.2). Ten years were correlated with a coefficient > 0.83 to zooMFA2 (Fig. 5c). Finally, the first two *PCs* of the SPF MFA

(referred to as spfMFA1 and spfMFA2 hereafter) explained 45.5 % of the space-time variance in the SPF biomass dataset (Fig. 4). Eleven years were correlated with a coefficient higher than the threshold (here set to 0.9, see Methods section 2.7.2) to the spfMFA1, and half the years (n = 8) were correlated to the spfMFA2 (Fig. 5d). Eventually, eight MFA *PCs* were retained as synthetic descriptors for the next steps of the analysis (*i.e.* hydroMFA1, hydroMFA2, hydroMFA3; phytoMFA1; zooMFA1, zooMFA2; spfMFA1, spfMFA2).

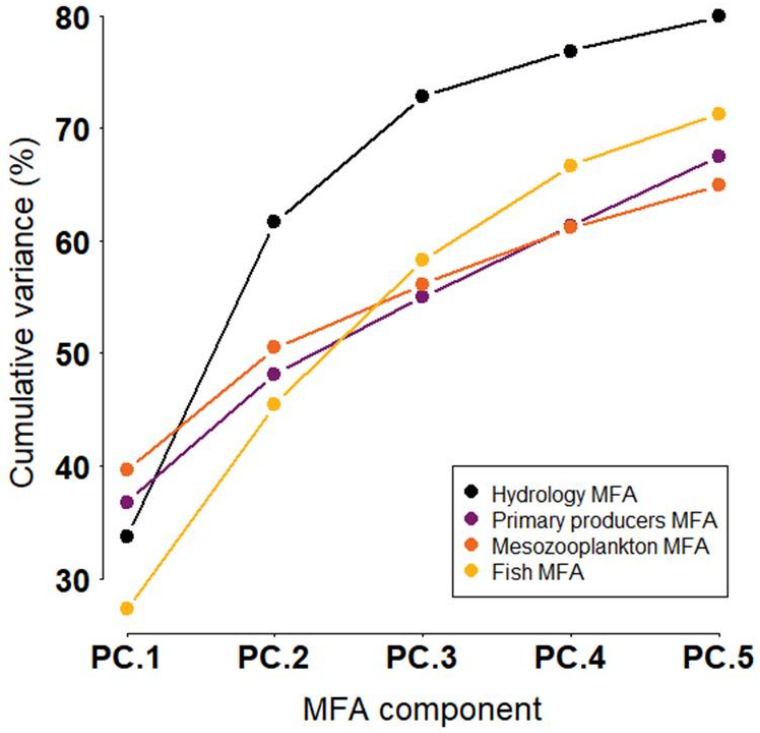


Fig. 4: Cumulative percentage of variance explained by the first five principal components of the Multiple Factor Analyses applied to the series of multivariate maps characterising hydrology, mesozooplankton and small pelagic fish (2004 - 2019) and primary producers data (2009 - 2019).

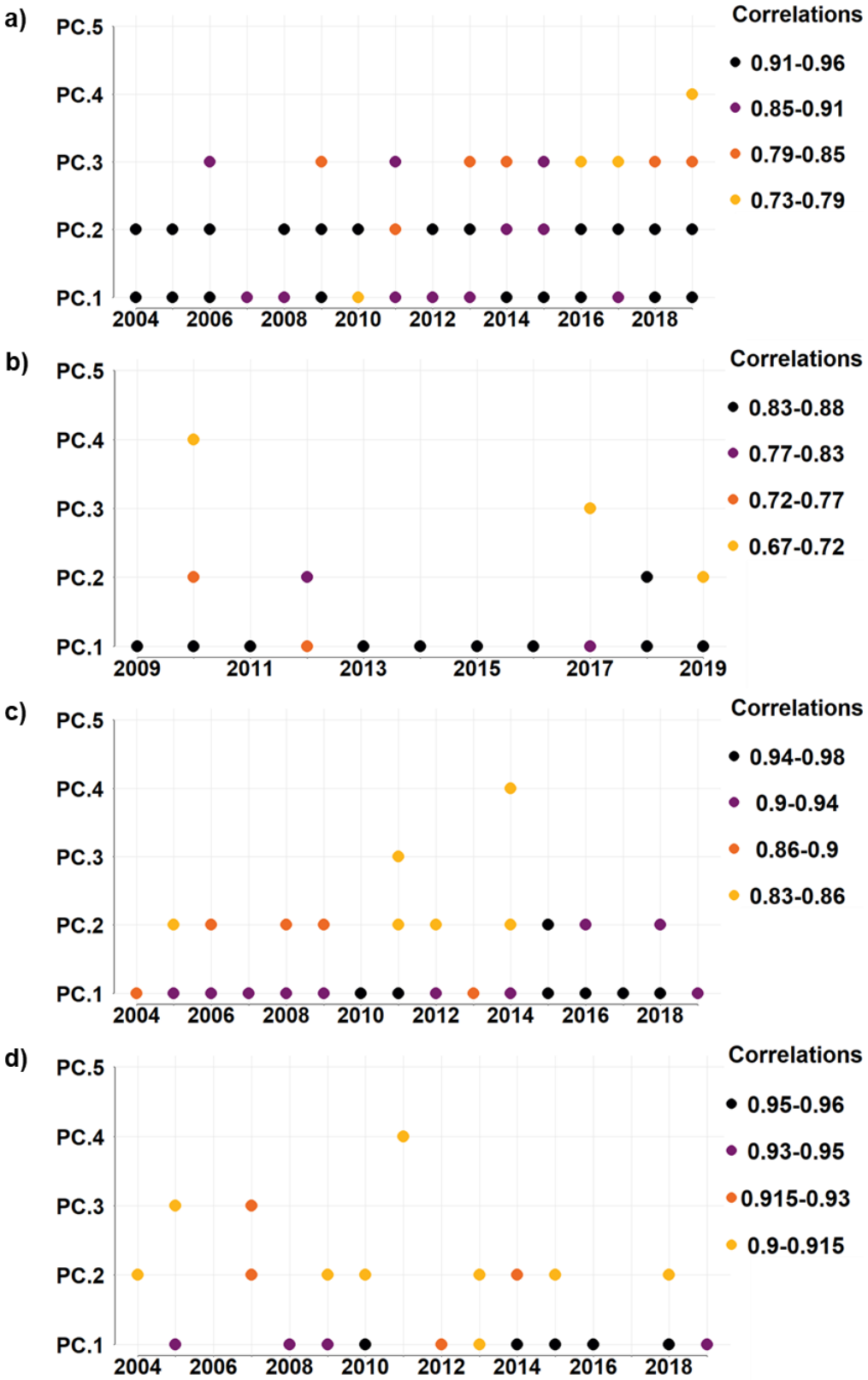


Fig. 5: Correlations between the years and the first five principal components of the Multiple Factor Analyses applied to the series of multivariate maps characterising (a) hydrology (2004 – 2019), (b) primary producers (2009 - 2019), (c) mesozooplankton (2004 – 2019) and (d) small pelagic fish (2004 - 2019). Only the correlations higher than the thresholds are shown (see Methods section 2.7.2).

## 3.3 Mesozooplankton ecosystem component

### *3.3.1 Mesozooplankton MFA selected PCs*

Here we present the spatial patterns (MFA *PCs*) in the mesozooplankton ecosystem component, based on the mapping of the mean individuals' (grid cells') coordinates in the mesozooplankton MFA factorial space (Fig. 6a and c). The variables defining the MFA *PCs* are shown in Fig. 6b and d.

The zooMFA1 showed a dominant coastal – offshore gradient in the mesozooplankton community. This structure was highlighted by the highest values in coastal areas, between the Loire estuary and the Arcachon Bay (Fig. 6a, lightest cells), and the lowest along the shelf break, north to 46°N (Fig. 6a, darkest cells). Small copepods, such as Acartiidae, Temoridae, Poecilostomatoida and Harpacticoida, as well as Cnidarians, Cladocerans, Bivalvia, Echinoderms and meroplanktonic crustaceans larvae groups displayed consistent positive correlations with zooMFA1 over the time series, revealing higher biomass in coastal areas. Significant positive correlations with zooMFA1, and consequently higher biomass in coastal areas, were also observed for appendicularians between 2005 and 2012 and between 2016 and 2019, indicating a higher variability across years for this taxon. On the contrary, Metridinidae, Euchaetidae, and to a lesser extent Calanidae showed consistent negative correlations with zooMFA1, and consequently high biomass offshore, especially north to 46°N (Fig. 6b).

The zooMFA2 revealed a North – South gradient, highlighted by the highest values in the northern part of the BoB along the Brittany southern coast (Fig. 6c, lightest cells), and the lowest ones in the south, especially over the shelf break, south to 45.5°N (Fig. 6c, darkest cells). The only taxa displaying a consistent positive correlation with this component were the meroplanktonic crustaceans larvae, after 2008 (Fig. 6d), showing higher biomass in the northern part of the BoB.

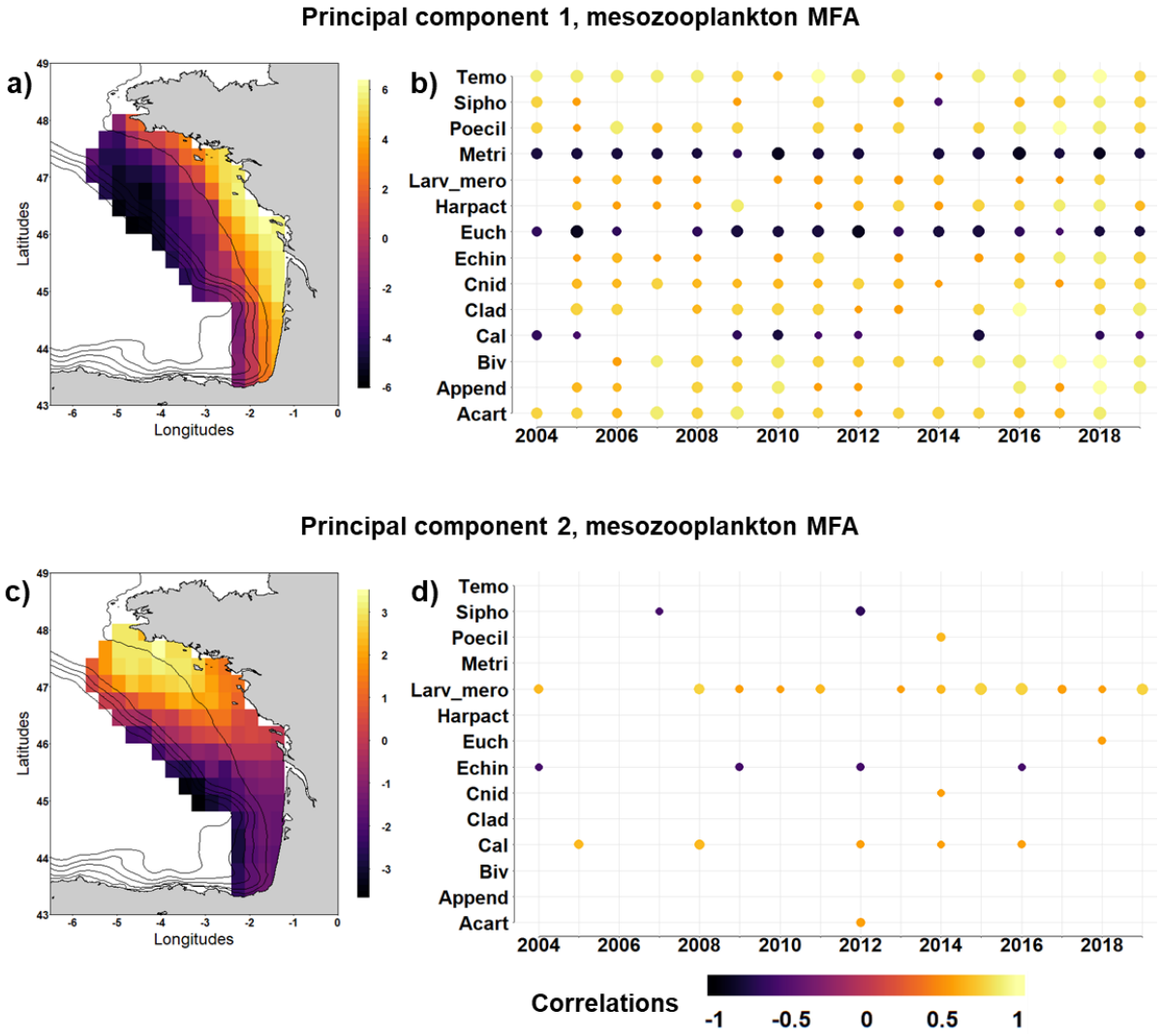


Fig. 6: Maps of mean individuals' (grid cells') coordinates on mesozooplankton Multiple Factor Analysis (MFA) principal component *PC.1* (a) and *PC.2* (c), and time series of significant correlations (> |0.5|) between the 24 taxonomic groups and MFA *PC.1* (b) and *PC.2* (d). The disk radii are proportional to the absolute value of the correlation coefficient. The mesozooplankton MFA was performed on the maps time series of 24 taxonomic groups biomass calculated from the PELGAS data, from 2004 to 2019 (Table 1).

### *3.3.2 Mesozooplankton zonation in the Bay of Biscay and its temporal evolution*

The hierarchical clustering of the mean individuals' (grid cells') coordinates in the MFA factorial space made by the two selected *PCs* (*i.e.* zooMFA1 and zooMFA2, explaining 50.5 % of the mesozooplankton dataset total variance, Fig. 4), resulted in identifying three clusters, on the basis of the classification tree presented in Fig. 7a and the Nbclust method to identify significant clusters (Fig. 7b). The clusters' spatial distribution and their variability in time are presented in Fig. 8.

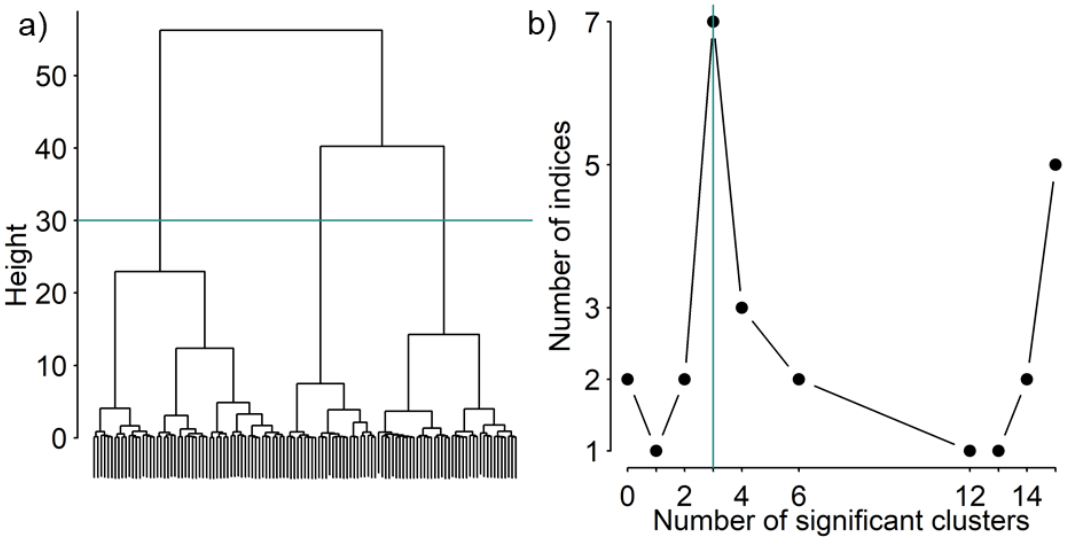


Fig. 7: (a) Classification tree of the hierarchical clustering of mean individuals (grid cells) coordinates in the mesozooplankton Multi Factor Analysis factorial space, made by the two selected mesozooplankton new descriptors (*i.e.* zooMFA1 and zooMFA2). (b) Number of clusters suggested by the Nbclust method (see section 2.7.3). Three clusters were retained (cut line in blue).

492

493 The time-consistent mesozooplankton spatial pattern combined coastal –
494 offshore and north – south gradients (Fig. 8a). A coastal cluster (G2, blue / medium
495 coloured cluster) extended from the Loire estuary to the south coast of the BoB, where
496 all taxa displayed higher-than-average biomass except large copepods (*i.e.* Calanidae,
497 Metridinidae and Euchaetidae) (Fig. 8c). A northern cluster (G3, yellow / light coloured
498 cluster) was located North of 45.5°N, from offshore waters along the shelf break to the
499 south Brittany coast. It was characterised mostly by Euchaetidae, and to a lesser extent
500 Metridinidae, Calanidae and meroplanktonic crustaceans' larvae, all of them showing
501 higher-than-average biomasses in this area (Fig. 8b). Finally, a southern cluster (G1,
502 purple / dark coloured cluster) extended from the central – shelf areas, south of 46°N,
503 mostly along the shelf break. Metridinidae dominated this southern mesozooplankton
504 community, and Appendicularians, Cladocerans, Echinodermata, Euchaetidae and
505 Siphonophorae also exhibited higher-than-average biomasses. On the contrary,
506 Cnidarians, meroplanktonic crustaceans' larvae and Temoridae displayed the lowest
507 overall biomass in this cluster (Fig. 8d). The spatial clusters corresponded to habitats
508 of particular communities that were consistent in time. The largest temporal variability
509 was located offshore in the northern cluster. The coastal and northern clusters covered

large spatial areas, whereas the southern cluster was less spatially extended and confined to the small southern outer-shelf and shelf break (Fig. 8a).

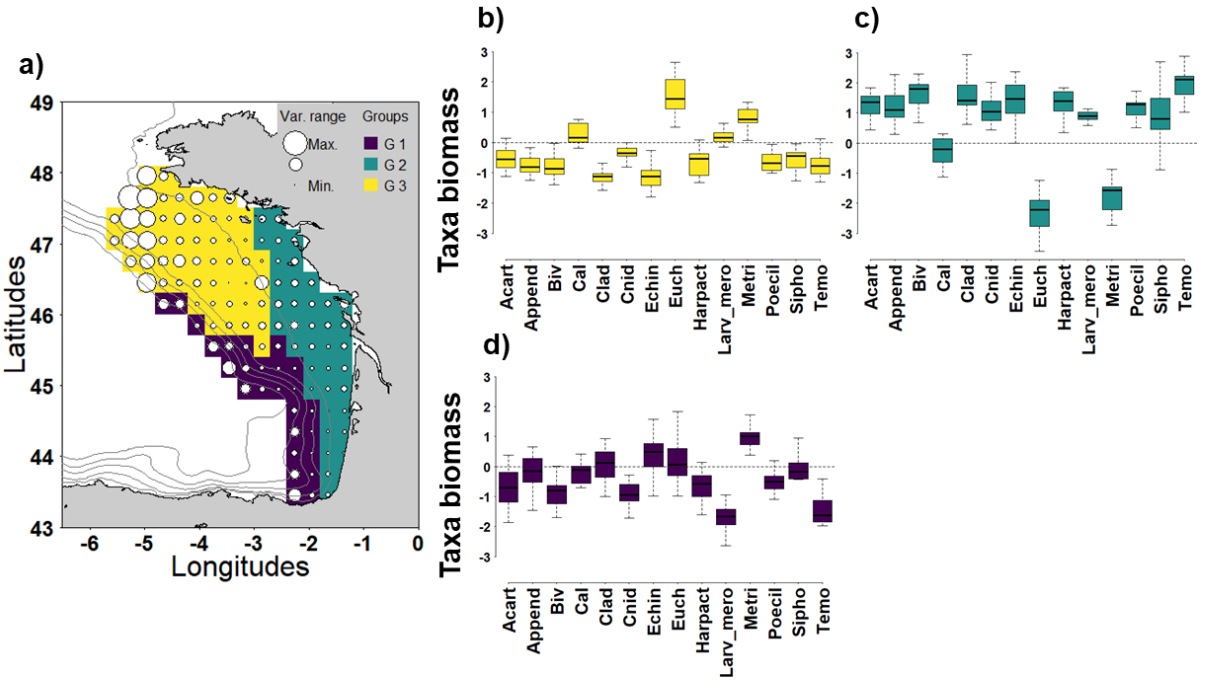


Fig. 8: (a) Time-consistent spatial patterns of the mesozooplankton community, derived from the hierarchical clustering of grid cells in the mesozooplankton Multiple Factor Analysis (MFA) space (two first principal components). White dots diameters are proportional to the inter-annual variability over the 16 years of the study. (b – d) Boxplots showing the inter-annual variability of the taxa biomasses (µg dry weight.m-3) in each cluster. The taxa shown are significantly correlated to the mesozooplankton MFA *PCs* with a frequency in time higher than 0.5. The horizontal dashlines mark the overall mean biomass (see Methods section 2.7.3).

Most of the grid cells within the coastal cluster G2 showed high occurrence frequencies in time (> 0.8), meaning that they consistently belonged to this cluster over time (Fig. 9c). The occurrence frequency of the grid cells within the southern and northern offshore clusters were smaller and more variable over years. Some grid cells along the shelf break between 46°N and 47°N switched between both clusters, depending on the year (Fig. 9a and b). The annual distributions of clusters can be found in the Appendix B, Fig. B1.

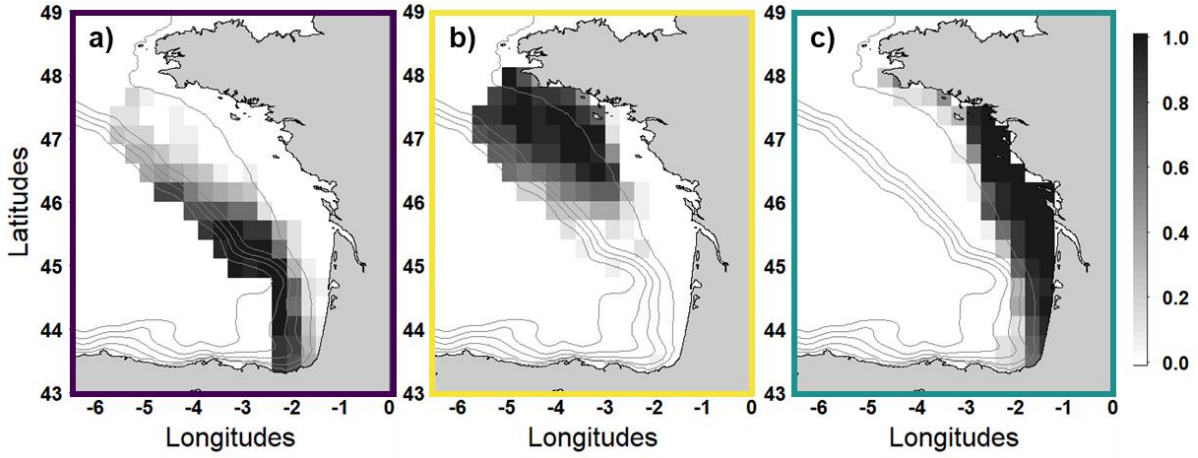


Fig. 9: Frequencies in time of grid cells' occurrences in each of the clusters forming the time-consistent spatial pattern: southern cluster G1 (a), northern cluster G3 (b), coastal cluster G2 (c).

## 3.4 Other ecosystem components MFA selected *PCs*

### *3.4.1 Hydrology ecosystem component*

Here we present the spatial patterns (MFA *PCs*) in the hydrology ecosystem component, based on the mapping of the mean individuals' (grid cells') coordinates in the hydrology MFA factorial space (Fig. 10a, c, e). The variables best correlated to the MFA *PCs* are shown in Fig. 10b, d, f.

The hydroMFA1 underpinned a dominant coastal – offshore gradient. This structure was highlighted by the lowest values off the Loire, Gironde and Adour estuaries (Fig. 10a, darkest cells) and the highest along the shelf break in the northern part of the BoB (Fig. 10a, lightest cells). The surface salinity and the mixed layer maximum depth had consistently positive correlations with hydroMFA1, meaning that these variables drove the coastal-offshore gradient of hydroMFA1 with the highest values located offshore in the northern part of the BoB between 2004 and 2019. On the contrary, the equivalent freshwater height was constantly negatively correlated with hydroMFA1, revealing the influence of the river plumes in coastal waters. Finally, surface temperature displayed negative correlations with hydroMFA1 at the beginning (from 2004 to 2008) and at the end (from 2014 to 2019) of the time series, suggesting that it contributed significantly to the coastal – offshore gradient those years, with higher values in coastal areas (Fig. 10b).

The hydroMFA2 displayed a north – south gradient, with the highest values in the southern part of the BoB (Fig. 10c, lightest cells) and the lowest values in the northern part of the BoB, along the Brittany southern coast, north to the Loire estuary (Fig. 10c, darkest cells). The constant positive correlations of both surface and bottom temperature with the hydroMFA2 throughout the series highlighted higher water temperatures, in the south of the BoB, and colder water temperatures in the north (Fig. 10d).

The potential energy deficit was the only variable significantly correlated to the hydroMFA3, with positive values (Fig. 10f), explaining the spatial pattern in hydroMFA3 with highest values in the middle of the shelf centered on the 100 m isobaths (Fig. 10e, lightest cells).

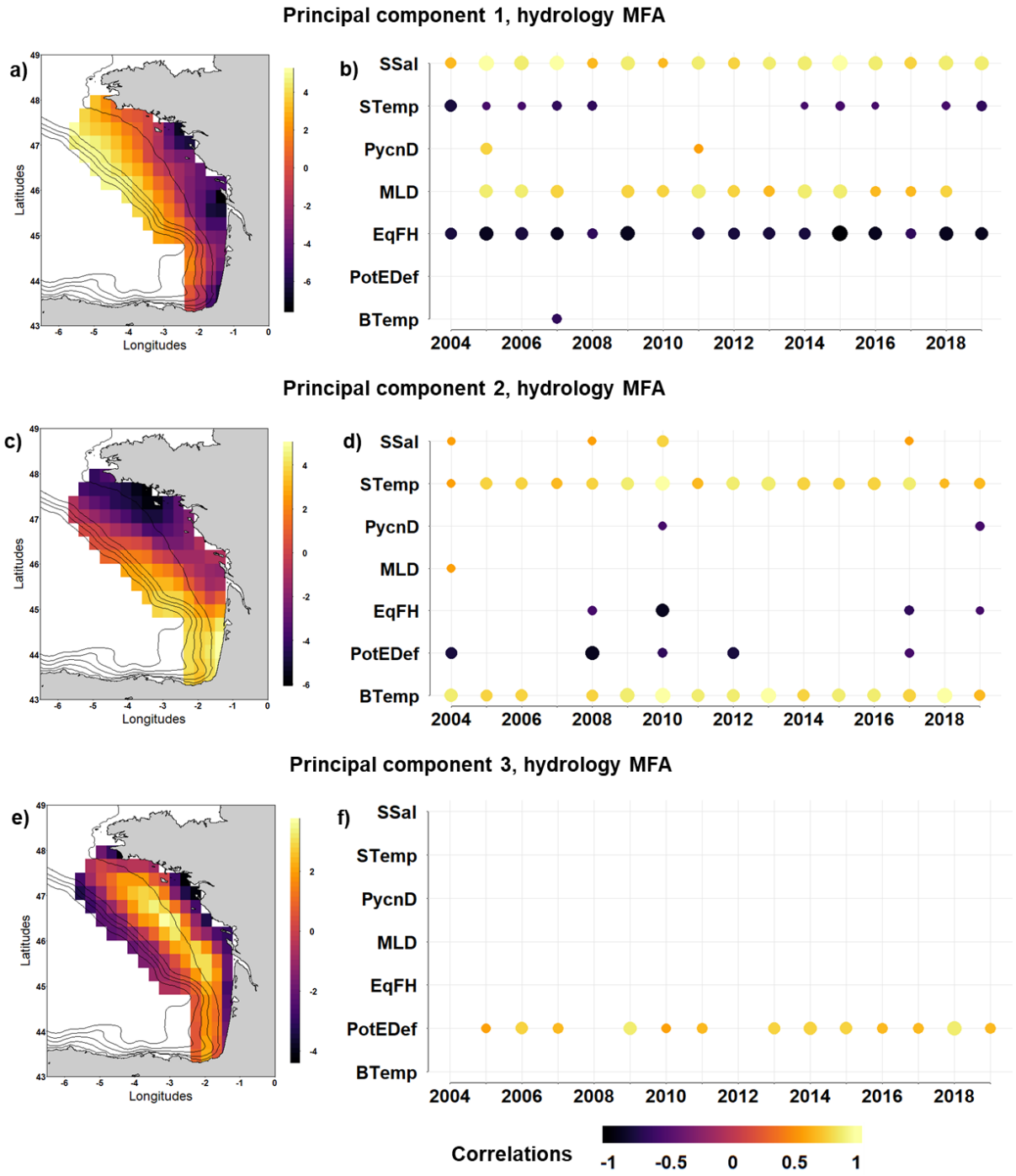


Fig. 10: Maps of mean individuals' (grid cells') coordinates on hydrology Multiple Factor Analysis (MFA) principal component (*PC*) 1 (a), 2 (c) and 3 (e), and time series of significant correlations (> |0.5|) between the seven hydrological parameters and the MFA *PC.1* (b), *PC.2* (d) and *PC.3* (f). The disk radii are proportional to the absolute value of the correlation coefficient. The hydrology MFA was performed on the maps time series of seven hydrological parameters derived from PELGAS and satellite data, from 2004 to 2019 (Table 2).

551

### *3.4.2 Primary producers ecosystem component*

Here we present the spatial patterns of the primary producers ecosystem component, based on the mapping of grid cells coordinates in the primary producers MFA factorial space (Fig. 11a). The variables best correlated with the MFA *PCs* are shown in Fig. 11b.

The phytoMFA1 exhibited a dominant coastal – offshore gradient. This structure was highlighted by the low values offshore, along the shelf break in the south of the BoB (Fig. 11a, darkest cells). High value were located in coastal areas, with highest values off the Loire estuary and to a lesser extent, off the Gironde and Adour estuaries (Fig. 11a, lightest cells). Surface chlorophyll-*a* concentrations of organisms larger than 20 µm, total surface chlorophyll-*a* concentrations and satellite-derived chlorophyll-*a* concentrations were consistently positively correlated to phytoMFA1, showing highest values in coastal areas, especially in the Loire estuary, between 2009 and 2019 (Fig. 11b). On the contrary, the depth of the chlorophyll maximum displayed negative correlations with phytoMFA1 approximately every other year, revealing higher values along the shelf break in the south and contributing significantly to the coastal-offshore gradient in 2009, 2011, 2013, 2015, 2016 and 2019 (Fig. 11b).

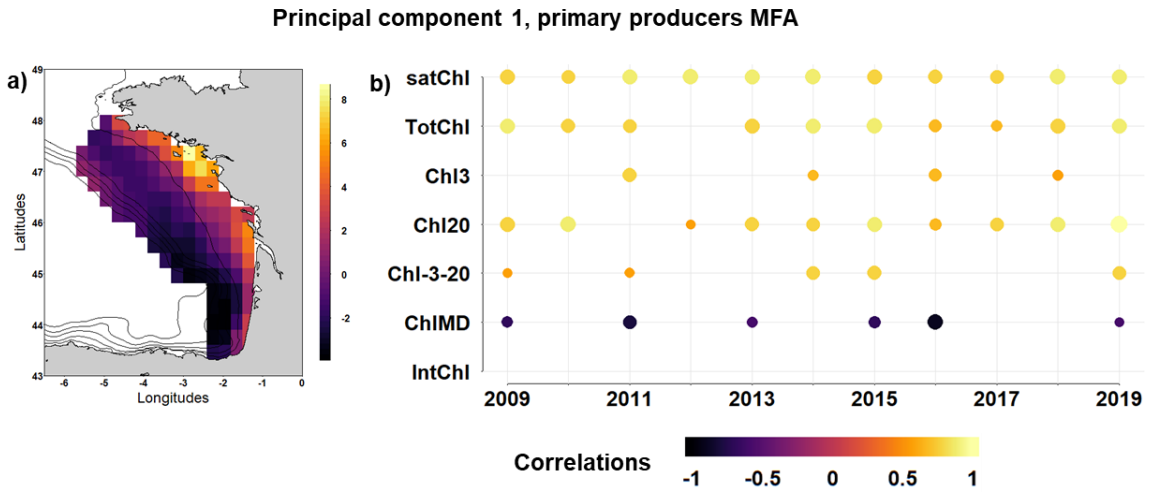


Fig. 11: Maps of mean individuals' (grid cells) coordinates on the primary producers Multiple Factor Analysis (MFA) principal component *PC.1* (a) and time series of significant correlations (> |0.5|) between the seven phytoplankton variables and *PC.1* (b). The disk radii are proportional to the absolute value of the correlation coefficient. The primary producers MFA was performed on the maps time series of chlorophyll-*a* parameters derived from PELGAS and satellite data, from 2009 to 2019 (Table 2).

### *3.4.3 Small pelagic fish ecosystem component*

Here we present the spatial patterns of the SPF ecosystem component, based on the mapping of grid cells coordinates in the SPF MFA factorial space (Fig. 12a). The variables best correlated with the MFA *PCs* are shown in Fig. 12b.

The spfMFA1 map showed a south-eastern – north-western gradient. This structure was underpinned by the lowest values offshore north to 45.5°N, along the shelf break (Fig. 12a, darkest cells), and the highest in the south-eastern part, from the Gironde estuary to 44.5°N (Fig. 12a, lightest cells). Small anchovy (*i.e.* ENGR-ENC. (10-15)), sardine (*i.e.* SARD-PIL.), sprat (*i.e.* SPRA-SPR.) and Atlantic chub mackerel (*i.e.* SCOM-COL.) of all sizes were positively correlated to spfMFA1 (Fig. 12b), displaying higher biomass in the south-eastern part of the BoB. Note this pattern is particularly consistent for large Atlantic chub mackerel after 2013 (six consecutive years for > 30 cm Atlantic chub mackerel). On the other hand, high biomass of blue whiting (*i.e.* MICR-POU) and large Atlantic horse mackerel (*i.e.* TRAC-TRU > 25 cm) were found offshore in the northern part of the BoB, showing negative correlations with spfMFA1, at the end of the time series (after 2014 and between 2013 and 2017, respectively) (Fig. 12b).

The spfMFA2 map showed an East – West gradient. This structure was underpinned by the low values in the coastal area, from 46°N to 47.5°N, including the Brittany southern coast (Fig. 12c, darkest cells), and high values in the southern part of the BoB and along the shelf break, south to 46°N (Fig. 12c, lightest cells). Sprat between 10 and 15 cm (*i.e.* SPRA-SPR. (10-15)) had consistent negative correlations with the spfMFA2, meaning that they had higher biomass in coastal areas. On the contrary, large Atlantic mackerel (> 30 cm) (*i.e.* SCOM-COL.) had positive correlations with the spfMFA2, showing higher biomass in the south. The same pattern was observed for large Atlantic chub mackerel before 2013 (Fig. 12d).

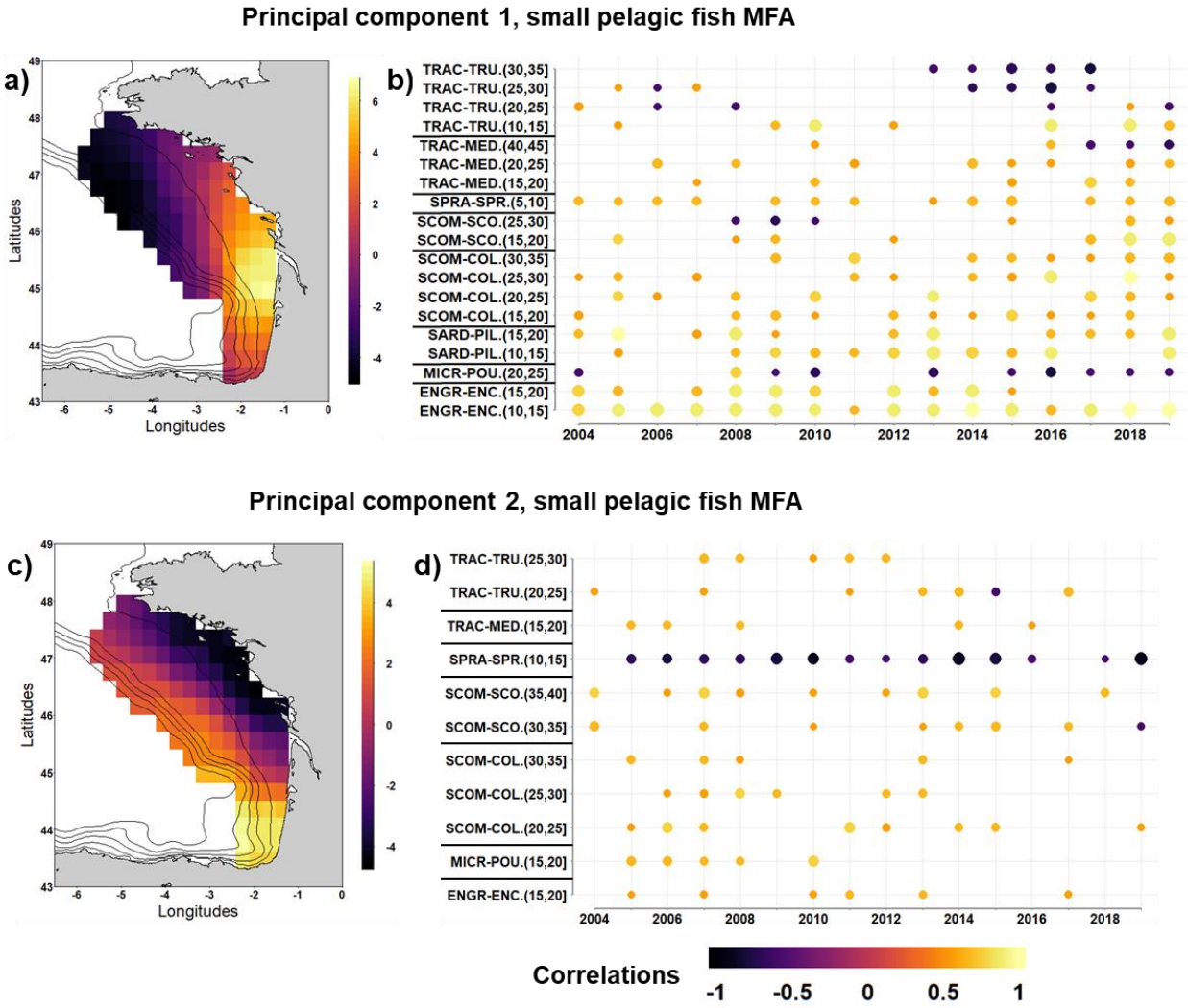


Fig. 12: Maps of mean individuals (grid cells) coordinates on small pelagic fish (SPF) Multiple Factor Analysis (MFA) principal component PC.1 (a) and PC.2 (c), and time series of significant correlations (> |0.5|) between the SPF species considered by 5 cm size classes and MFA PC.1 (b) and PC.2 (d). The disk radii are proportional to the absolute value of the correlation coefficient. The small pelagic fish MFA was performed on the maps time series of SPF species biomass considered by 5 cm size classes, calculated from the PELGAS data, from 2004 to 2019 (Table 3).

## 3.5 Correlates of the observed mesozooplankton space-time patterns

We searched for correlates of the mesozooplankton main space-time patterns (zooMFA1 and zooMFA2) using GLMs. We used the six selected *PCs* in the hydrology, primary producers and SPF MFA as predictors.

### *3.5.1 First PC in the mesozooplankton space-time pattern: zooMFA1*

For the initial full model built with the six predictors, all the VIF values were higher than five (except that of hydroMFA3, VIF value = 3.7), showing collinearity between all the predictors except hydroMFA3 (Appendix C, Table C.1). The predictors phytoMFA1 and spfMFA2 had highest linear correlation coefficient with the other predictors (Appendix C, Fig. C.1) and were thus removed from the initial full model. The model without these two predictors showed acceptable VIF values and thus the predictors hydroMFA1, hydroMFA2, hydroMFA3 and spfMFA1 were kept for the subsequent model selection procedure.

The stepwise backward model selection procedure showed that the four predictors together constituted the best model explaining the zooMFA1 (lowest AIC, Appendix C, Table C.2). The salinity and water column stratification gradient (hydroMFA1, Fig. 5a and b) explained most of the variance in the model. To a lesser extent, the North - South gradient in the water temperature (hydroMFA2, Fig. 5c and d) and SPF biomass spatial patterns (spfMFA1, Fig. 12a and b) were also significant contributors explaining the mesozooplankton coastal-offshore gradient (zooMFA1, Fig. 8a and b) (Table 4). On the other hand, the potential energy deficit spatial pattern (hydroMFA3, Fig. 5e and f) was not significant in the model (Table 4), but a model without this predictor was not significantly different from the best model, as their AIC difference was smaller than two (Appendix C, Table C.2).

Table 4: Predictors included in the model explaining the first principal component of the mesozooplankton MFA, with the estimated coefficients (“Estimate” and “Std. Error”) and their significance in the model (“P value”).

| Parameters | Estimate | Std. Error | P value |
|---|---|---|---|
| (Intercept) | 2.49 | 0.17 | < 2e-16 *** |
| hydroMFA1 | -0.093 | 0.015 | 4.88e-09 *** |
| hydroMFA2 | -0.047 | 0.009 | 2.55e-06 *** |
| hydroMFA3 | -0.023 | 0.012 | 0.07 |
| spfMFA1 | 0.088 | 0.015 | 8.79e-08 *** |

### *3.5.2 Second PC in the mesozooplankton space-time pattern: zooMFA2*

Using the same procedure as previously (VIF value of the predictors in the initial full model and correlation coefficients among predictors, see Appendix C, Table C.1 and Fig. C.1), the predictors hydroMFA1, phytoMFA1 and spfMFA2 were removed from the analysis.

The stepwise backward model selection procedure was applied with the three selected predictors (*i.e.* hydroMFA2, hydroMFA3 and spfMFA1). The best model explaining zooMFA2 included hydroMFA2 and spfMFA1 (lowest AIC, Appendix C, Table C.3) but hydroMFA2 as the only significant predictor (Table 5). The map of zooMFA2 was underpinned by the North – South gradient in the biomass of meroplanktonic crustaceans larvae (zooMFA2, Fig. 8c and d). Thus, this structuration followed the North – South gradient in water temperature (hydroMFA2, Fig. 5c and d). Both predictors hydroMFA3 and spfMFA1 were not significantly explicative in the model (Table 5), but models without those predictors were not significantly different, as their AIC difference was smaller than two (Appendix C, Table C.3). This suggested that the potential energy deficit (hydroMFA3) and the SPF biomass spatial patterns (spfMFA1) were less influential in structuring in the mesozooplankton North – South gradient (zooMFA2).

Table 5: Predictors included in the model explaining the second principal component of the mesozooplankton MFA, with the estimated coefficients (“Estimate” and “Std. Error”) and their significance in the model (“P value”).

| **Parameters** | **Estimate** | **Std. Error** | **P value** |
|---|---|---|---|
| (Intercept) | 2.35 | 0.063 | < 2e-16 *** |
| hydroMFA2 | -0.13 | 0.006 | < 2e-16 *** |
| hydroMFA3 | 0.007 | 0.009 | 0.434 |
| spfMFA1 | -0.008 | 0.005 | 0.113 |

# 4 Discussion

This study is the first space-time characterisation of mesozooplankton springtime assemblages, over the BoB continental shelf and almost two decades. Results show that the spatial patterns in the mesozooplankton assemblage was coherent with that observed in other pelagic ecosystem components (hydrology, primary producers and small pelagic fish). Coastal-offshore and North-South gradients were the main mesoscale spatial patterns. Small copepods, gelatinous and meroplanktonic organisms characterised coastal areas. Euchaetidae and meroplanktonic crustaceans' larvae showed higher biomass in the northern part of the BoB while Metridinidae, Cladocera, Appendicularia and Echinodermata had higher biomass in the southern part. Moreover, the high correlations between the years and the mesozooplankton MFA *PCs* underlined the stability in time of the above-mentioned spatial patterns. The high occurrence frequencies of grid cells to the clusters defining specific regions in the BoB evidenced the temporal consistency of the mesozooplankton assemblage spatial structure. In the other pelagic ecosystem components taken into account, salinity, water column stratification and primary producers supported a coastal-offshore gradient, while surface and bottom water temperature drew a North-South gradient. In addition, the spatial structure in the SPF biomass by size classes obtained here was consistent with that obtained by Doray et al. (2018) with a similar methodology. Finally, the observed mesozooplankton patterns were correlated with those of hydrology and SPF ecosystem components.

## 4.1 Mesozooplankton assemblages temporal stability

The highest inter-annual variability occurred offshore in the northern part of the BoB, where some grid cells had missing data at the beginning of the time series. Therefore, this result can be due to the missing data imputation in this area. Yet, a true biological variability in the mesozooplankton assemblage could also be real close to the shelf break. The consistency in time of the mesozooplankton assemblage was a conclusion drawn by Irigoien et al. (2008), studying spring zooplankton distribution between 1998 and 2006 in the southern part of the BoB. Feuilloley et al. (2022) also showed the high stability through time of the zooplankton density, body size and taxonomic composition in the North Western Mediterranean Sea, during the period 1995-2019. Yet, abrupt

shifts in community structure could be expected when analysing long-term dynamics in the context of environmental changes. Such regime shifts were detected in the late 1980s and in the 1990s in several marine regions in the Northern Hemisphere (Beaugrand et al., 2015; Morse et al., 2017; Bode et al., 2020; Chust et al., 2022). Recently, Dessier et al. (2018) found a change in the large copepod species dominance in the South of the BoB between the period 2003 – 2006 and the period 2007 – 2009, preceding a return toward the initial situation over the period 2010 – 2013. Also, Iriarte et al. (2022) distinguished three periods in the relative density of copepod species in the Southeastern BoB: 1998 – 2007, 2008 – 2013 and 2014 – 2015. Here, the mesozooplankton community was studied using 24 taxonomic groups, a less detailed level than the species level used in these previous studies. Fine taxonomic resolution could reveal shifts in species dominance that could compensate each other when analysing the community at a broader taxonomic resolution and, consequently, the overall structure could appear consistent in time. This point constitutes a potential limit of our study. Shifts in species dominance could have occurred in the zooplankton community between 2004 and 2019 but the broad taxonomic resolution used here may not have enable the observation of such possible changes, resulting in an apparent temporal stability over the time series. On the other hand, these studies were done at a smaller spatial scale (southern part of the BoB in Dessier et al. (2018); two neritic stations in the Cantabrian Sea in Iriarte et al. (2022)), and the shifts occurring in restricted areas could be undetectable at a broader spatial scale or not affect the large scale distribution pattern.

## 4.2 Coherent spatial patterns across pelagic ecosystem components

Our results agreed with the spatial organisation in mesozooplankton assemblages along a coastal-offshore gradient previously showed in the BoB (Albaina and Irigoien, 2004, 2007a; Sourisseau and Carlotti, 2006; Irigoien et al., 2008; Vandromme et al., 2014; Dessier et al., 2018) and in other shelf ecosystems (Marcolin et al., 2013; Pepin et al., 2015; Noyon et al., 2022). Our study also confirms that surface and bottom water temperature, salinity-related parameters and water column stratification indices were key hydrographic variables that correlated with this mesozooplankton springtime spatial structure (Albaina and Irigoien, 2004; Zarauz et al., 2007; Irigoien et al., 2011;

Dessier et al., 2018; Iriarte et al., 2022). Hydrological parameters integrating the historical seasonal conditions, such as the equivalent freshwater height, mixed layer depth and the deficit of potential energy, were key variables to study the mesozooplankton spring habitat, taking into account the onset of spring conditions. The correlations between the hydrology and primary producers space-time patterns observed here confirm the important role of nutrients enrichment at the rivers' mouths in the primary producers development in spring in the BoB (Guillaud et al., 2008). Primary producers are known to drive the mesozooplankton dynamics in the BoB (Zarauz et al., 2008; Dessier et al., 2018; Iriarte et al., 2022) and elsewhere (Pepin et al., 2015; Capuzzo et al., 2018). Here, because of the method used, the primary producers' space-time pattern was not included in the models to explain the mesozooplankton space-time structure. Yet, the correlations between the hydrology and primary producers ecosystem components (Appendix C, Fig. C.1) combined with the hydrology space-time patterns significance in the linear models (Tables 4 and 5) suggest that the hydrological landscapes may influenced the mesozooplankton community structure through the primary production and trophic relationships between phytoplankton and mesozooplankton in the BoB.

The North-South gradient in the mesozooplankton assemblage in the BoB was never described before, as previous studies mostly focused on the southern part of the BoB (Albaina and Irigoien, 2004, 2007a; Irigoien et al., 2008; Dessier et al., 2018). At the scale of the Northeast Atlantic, a strong latitudinal effect potentially driven by temperature regimes has been shown on the seasonal and interannual variability of two copepod species (Valdes et al., 2022). Moreover, Fanjul et al. (2019) demonstrated that some zooplankton groups' abundances displayed temperature-mediated latitudinal differences, and that meroplankton contributed more than holoplankton to the main between-site differences. In the BoB, the spring meroplanktonic crustaceans' larvae distribution could be driven by the temperature-induced latitudinal gradient, resulting in higher biomass in the northern coastal area. Nevertheless, this result could also highlight the timing of the surveys, lasting one month and starting in the south of the BoB, potentially before the development of the meroplanktonic crustaceans' larvae in this area.

Furthermore, the correlation between mesozooplankton and SPF spatial patterns confirms the consistent spatial structure across pelagic ecosystem components that

743 have been reported in the BoB (Doray et al., 2018a; Petitgas et al., 2018), possibly
744 mediated via predation and/or forced by hydrological structuring. For example, taking
745 into account the eight major SPF species inhabiting the BoB, Bachiller and Irigoien
746 (2015) described an overall high diet overlap and concluded to a top – down control by
747 these planktivorous fishes on zooplankton. Elsewhere, such links between ecosystem
748 components were highlighted in the Mediterranean Sea (Feuilloley et al., 2020), on the
749 Portuguese continental coast (Fonseca et al., 2022), in the North Sea (Capuzzo et al.,
750 2018) and in Barents Sea (Stige et al., 2014). Here, the spatial structures in the
751 hydrological parameters, primary producers and SPF were similar to that in
752 mesozooplankton assemblages and were also consistent in time. Spatial structures
753 had been described for different ecosystem components in the BoB (Special Issue No.
754 166 in Progress in Oceanography, 2018), including river plumes, primary producers,
755 fish and top-predators but this is the first time they are described for the
756 mesozooplankton and shown to be similar to the other ecosystem components. Such
757 consistency in the spatial structure across ecosystem components and over time is
758 remarkable. Donohue et al. (2013) discussed the multiple and related facets of
759 ecosystem stability. In the case of the BoB continental shelf at springtime, hydrographic
760 landscapes resulting from river plumes' extents on the shelf and temperature gradients
761 (Koutsikopoulos and Le Cann, 1996; Koutsikopoulos et al., 1998; Castaing et al., 1999;
762 Planque et al., 2004; Guillaud et al., 2008) certainly impede strong structuring meso-
763 scale forcings on the BoB regional pelagic ecology. The structure could also be
764 maintained and reinforced by top-down and bottom-up controls through trophic levels
765 as generally reported for the North Atlantic (Frank et al., 2007) although not directly
766 studied here.

## 767 4.3 Data and methods used

768 Such regional study linking several ecological components was made possible by
769 the unique long-term and spatially resolved datasets constructed from integrated
770 surveys. Thus, maintaining such surveys is of primary importance for ecosystem
771 assessment research, especially in the context of climate change, as they provide a
772 platform dedicated to gather data from several biological and abiotic components at
773 the same temporal and spatial resolution (Kupschus et al., 2016; Doray et al., 2018c).
774 Nevertheless, it should be noted that these *in situ* data sets provide a temporal

snapshot of the ecosystem state at the time of the surveys. Any apparent interannual variability could be caused by interannual differences in the seasonal evolution of the system (Huret et al., 2018). The combination of imaging and deep learning tools provided an efficient method to analyse a high quantity of mesozooplankton samples quickly and in a standardized way. This analytical pipeline, including also automated procedures for spatial gridding and missing data imputation, allowed to construct a mesozooplankton spatially resolved time series over 16 years. Finally, the MFA was well suited to estimate time-average spatial patterns in a multivariate dataset and perhaps less designed to evidence temporal trends in the mean distribution, at least in the way we implemented the method. Moreover, the results showing consistency in time of the spatial patterns were based on a subset of MFA principal components, accounting only for part of the total variance. The residual variance, not fully explained here, showed exceptional events, which we did not fully explore. Yet, the major time variations happened in particular years (for example, lowest mesozooplankton biomass in 2011 and 2015, Fig. 3) and were located in particular areas (offshore in the northern part of the BoB, Fig. 8), suggesting no obvious trend in time.

# 5 Conclusion

Thanks to long-term spatially resolved time series, we provided the first space-time characterisation of mesozooplankton springtime assemblage, correlated with other pelagic ecosystem components (hydrology, primary producers and SPF), over 16 years and the whole BoB continental shelf. We demonstrated coherent spatial patterns across pelagic ecosystem components supported by coastal-offshore and North-South gradients. Moreover, we highlighted the remarkable stability in time of these spatial patterns. The springtime spatial structure of biotic components seems to be based on spring hydrological landscapes and is potentially related to bottom-up and top-down trophic controls, although a more detailed study on the ecosystem components' correlations is needed to fully confirm this hypothesis. Our regional study relies on long-term spatially resolved datasets originating from integrated surveys and provide key understanding of the ecosystem structure and dynamics. Therefore, our work emphasize the importance of such surveys for ecosystem assessment research especially in the context of climate change.

# 6 Acknowledgements

The authors acknowledge receiving funding from the Ifremer DEFIPEL project France Filière Pêche projet d'avenir. NG acknowledges being funded by Region Pays de la Loire, FR and Ifremer. The authors wish to thanks the following technicians and engineers for their decisive contribution to the sample and data acquisition: P. Pineau (La Rochelle University), primary producers sampling and data acquisition; S. Le Mestre (Ifremer), zooplankton sampling lab work on board and ZooCAM management on land; P. Bourriau (Ifremer): zooplankton sampling and wet lab management on board and on land; B. Forest (Ifremer), design and development of ZooCAM software; A. Nowazcyk (PlanktonLab and University of Bordeaux) and the PIQV team (Sorbonne Université – CNRS), expertise in zooplankton identification. The authors wish also to thank the many other students, technicians and scientists who participated in the sampling and samples management on board and on land, and the successive crews of the R/V Thalassa involved in the PELGAS cruises from 2004 to 2019.

# 7 Authors contributions

NG: conceptualized the study, generated and scrutinized the imaging data, conducted the numerical analyses, drafted the paper. J-BR: conceptualized the study, supervised NG work, scrutinized the imaging data, drafted the paper. CD: conceptualized the study, supervised NG work, drafted the paper. MD: supervised numerical analyses and provided fish data, participated in the drafting. MH: provided hydrology data, participated in the drafting. PP: conceptualized the study, supervised NG work, drafted the paper. All co-authors reviewed and revised the paper before submission.

# 8 References


Abdi, H., Williams, L.J., Valentin, D., 2013. Multiple factor analysis: principal component analysis for multitable and multiblock data sets: Multiple factor analysis. Wiley Interdiscip. Rev. Comput. Stat. 5, 149–179. https://doi.org/10.1002/wics.1246

Albaina, A., Irigoien, X., 2007a. Fine scale zooplankton distribution in the Bay of Biscay in spring 2004. J. Plankton Res. 29, 851–870. https://doi.org/10.1093/plankt/fbm064

Albaina, A., Irigoien, X., 2007b. Zooplankton communities and oceanographic structures in a high-resolution grid in the south-eastern corner of the Bay of Biscay. Estuar. Coast. Shelf Sci. 75, 433–446. https://doi.org/10.1016/j.ecss.2007.05.028

Albaina, A., Irigoien, X., 2004. Relationships between frontal structures and zooplankton communities along a cross-shelf transect in the Bay of Biscay (1995 to 2003). Mar. Ecol. Prog. Ser. 284, 65–75. https://doi.org/10.3354/meps284065

Bachiller, E., Irigoien, X., 2015. Trophodynamics and diet overlap of small pelagic fish species in the Bay of Biscay. Mar. Ecol. Prog. Ser. 534, 179–198. https://doi.org/10.3354/meps11375

Banse, K., 1995. Zooplankton: Pivotal role in the control of ocean production: I. Biomass and production. ICES J. Mar. Sci. 52, 265–277. https://doi.org/10.1016/1054-3139(95)80043-3

Batchelder, H.P., Mackas, D.L., O'Brien, T.D., 2012. Spatial–temporal scales of synchrony in marine zooplankton biomass and abundance patterns: A world-wide comparison. Prog. Oceanogr. 97–100, 15–30. https://doi.org/10.1016/j.pocean.2011.11.010

Beaugrand, G., Conversi, A., Chiba, S., Edwards, M., Fonda-Umani, S., Greene, C., Mantua, N., Otto, S.A., Reid, P.C., Stachura, M.M., Stemmann, L., Sugisaki, H., 2015. Synchronous marine pelagic regime shifts in the Northern Hemisphere. Philos. Trans. R. Soc. B Biol. Sci. 370, 20130272. https://doi.org/10.1098/rstb.2013.0272

Bellier, E., Planque, B., Petitgas, P., 2007. Historical fluctuations in spawning location of anchovy (Engraulis encrasicolus) and sardine (Sardina pilchardus) in the Bay of Biscay during 1967–73 and 2000–2004. Fish. Oceanogr. 16, 1–15. https://doi.org/10.1111/j.1365-2419.2006.00410.x

Bode, A., Álvarez, M., García García, L.M., Louro, M.Á., Nieto-Cid, M., Ruíz-Villarreal, M., Varela, M.M., 2020. Climate and Local Hydrography Underlie Recent Regime Shifts in Plankton Communities off Galicia (NW Spain). Oceans 1, 181–197. https://doi.org/10.3390/oceans1040014

Burnham, K.P., Anderson, D.R., Burnham, K.P., 2002. Model selection and multimodel inference: a practical information-theoretic approach, 2nd ed. ed. Springer, New York.

Capuzzo, E., Lynam, C.P., Barry, J., Stephens, D., Forster, R.M., Greenwood, N., McQuatters-Gollop, A., Silva, T., van Leeuwen, S.M., Engelhard, G.H., 2018. A decline in primary production in the North Sea over 25 years, associated with reductions in zooplankton abundance and fish stock recruitment. Glob. Change Biol. 24, e352–e364. https://doi.org/10.1111/gcb.13916

Castaing, P., Froidefond, J.M., Lazure, P., Weber, O., Prud'homme, R., Jouanneau, J.M., 1999. Relationship between hydrology and seasonal distribution of suspended sediments on the continental shelf of the Bay of Biscay. Deep Sea Res. Part II Top. Stud. Oceanogr. 46, 1979–2001. https://doi.org/10.1016/S0967-0645(99)00052-1

Charrad, M., Ghazzali, N., Boiteau, V., Niknafs, A., 2014. NbClust: An R Package for Determining the Relevant Number of Clusters in a Data Set. J. Stat. Softw. 61, 1–36. https://doi.org/10.18637/jss.v061.i06

Chust, G., González, M., Fontán, A., Revilla, M., Alvarez, P., Santos, M., Cotano, U., Chifflet, M., Borja, A., Muxika, I., Sagarminaga, Y., Caballero, A., de Santiago, I., Epelde, I., Liria, P., Ibaibarriaga, L., Garnier, R., Franco, J., Villarino, E., Irigoien, X., Fernandes-Salvador, J.A., Uriarte, Andrés, Esteban, X., Orue-Echevarria, D., Figueira, T., Uriarte, Adolfo, 2022. Climate regime shifts and biodiversity redistribution in the Bay of Biscay. Sci. Total Environ. 803, 149622. https://doi.org/10.1016/j.scitotenv.2021.149622

Colas, F., Tardivel, M., Perchoc, J., Lunven, M., Forest, B., Guyader, G., Danielou, M.M., Le Mestre, S., Bourriau, P., Antajan, E., Sourisseau, M., Huret, M., Petitgas, P., Romagnan, J.B., 2018. The ZooCAM, a new in-flow imaging system for fast onboard counting, sizing and classification of fish eggs and metazooplankton. Prog. Oceanogr., Multidisciplinary integrated surveys 166, 54–65. https://doi.org/10.1016/j.pocean.2017.10.014

Cury, P., Bakun, A., Crawford, R.J.M., Jarre, A., Quiñones, R.A., Shannon, L.J., Verheye, H.M., 2000. Small pelagics in upwelling systems: patterns of interaction and structural changes in “wasp-waist” ecosystems. ICES J. Mar. Sci. 57, 603–618. https://doi.org/10.1006/jmsc.2000.0712

Dessier, A., Bustamante, P., Chouvelon, T., Huret, M., Pagano, M., Marquis, E., Rousseaux, F., Pignon-Mussaud, C., Mornet, F., Bréret, M., Dupuy, C., 2018. The spring mesozooplankton variability and its relationship with hydrobiological structure over year-to-year changes (2003–2013) in the southern Bay of Biscay (Northeast Atlantic). Prog. Oceanogr., Multidisciplinary integrated surveys 166, 76–87. https://doi.org/10.1016/j.pocean.2018.04.011

Donohue, I., Petchey, O.L., Montoya, J.M., Jackson, A.L., McNally, L., Viana, M., Healy, K., Lurgi, M., O’Connor, N.E., Emmerson, M.C., 2013. On the dimensionality of ecological stability. Ecol. Lett. 16, 421–429. https://doi.org/10.1111/ele.12086

Doray, M., Boyra, G., van der Kooij, J., 2021. ICES Survey Protocols - Manual for acoustic surveys coordinated under ICES Working Group on Acoustic and Egg Surveys for Small Pelagic Fish (WGACEGG). https://doi.org/10.17895/ICES.PUB.7462

Doray, M., Duhamel, E., Boiron-Leroy, A., Marchand, L., Bled--Defruit, G., Petitgas, P., 2022. Mean length and weight at-age of anchovy and sardine estimated during the PELGAS survey in the Bay of Biscay in springtime. https://doi.org/10.17882/88357

Doray, M., Hervy, C., Huret, M., Petitgas, P., 2018a. Spring habitats of small pelagic fish communities in the Bay of Biscay. Prog. Oceanogr., Multidisciplinary integrated surveys 166, 88–108. https://doi.org/10.1016/j.pocean.2017.11.003

Doray, M., Petitgas, P., Huret, M., Duhamel, E., Romagnan, J.B., Authier, M., Dupuy, C., Spitz, J., 2018b. Monitoring small pelagic fish in the Bay of Biscay ecosystem, using indicators from an integrated survey. Prog. Oceanogr., Multidisciplinary integrated surveys 166, 168–188. https://doi.org/10.1016/j.pocean.2017.12.004

Doray, M., Petitgas, P., Romagnan, J.B., Huret, M., Duhamel, E., Dupuy, C., Spitz, J., Authier, M., Sanchez, F., Berger, L., Dorémus, G., Bourriau, P., Grellier, P., Massé, J., 2018c. The PELGAS survey: Ship-based integrated monitoring of the Bay of Biscay

pelagic ecosystem. Prog. Oceanogr., Multidisciplinary integrated surveys 166, 15–29. https://doi.org/10.1016/j.pocean.2017.09.015

Doray, M., Petitgas, P., Saraux, C., Cornou, A.-S., 2013. EchoR: R Package for Computing Indices of the State of Fish Population and Communities, based on Fisheries Acoustic Data, R Package. Ifremer 10.

Escofier, B., Pagès, J., 1994. Multiple factor analysis (AFMULT package). Comput. Stat. Data Anal. 18, 121–140. https://doi.org/10.1016/0167-9473(94)90135-X

Fanjul, A., Iriarte, A., Villate, F., Uriarte, I., Artiach, M., Atkinson, A., Cook, K., 2019. Latitude, distance offshore and local environmental features as modulators of zooplankton assemblages across the NE Atlantic Shelves Province. J. Plankton Res. 41, 293–308. https://doi.org/10.1093/plankt/fbz015

Feuilloley, G., Fromentin, J.-M., Saraux, C., Irisson, J.-O., Jalabert, L., Stemmann, L., 2022. Temporal fluctuations in zooplankton size, abundance, and taxonomic composition since 1995 in the North Western Mediterranean Sea. ICES J. Mar. Sci. 79, 882–900. https://doi.org/10.1093/icesjms/fsab190

Feuilloley, G., Fromentin, J.-M., Stemmann, L., Demarcq, H., Estournel, C., Saraux, C., 2020. Concomitant changes in the environment and small pelagic fish community of the Gulf of Lions. Prog. Oceanogr. 186, 102375. https://doi.org/10.1016/j.pocean.2020.102375

Fonseca, P., Silva, A.D., Angélico, M.M., Garrido, S., 2022. Seasonal and spatial variability of Atlanto-Iberian pelagic fish diet with estimates of intraguild predation. Mar. Ecol. Prog. Ser. 687, 95–111. https://doi.org/10.3354/meps14011

Fox, J., Monette, G., 1992. Generalized Collinearity Diagnostics. J. Am. Stat. Assoc. 87, 178–183. https://doi.org/10.1080/01621459.1992.10475190

Fox, J., Weisberg, S., 2019. An R Compagnion to Applied Regression. Sage Thousand Oaks CA Third Edition.

Frank, K.T., Petrie, B., Shackell, N.L., 2007. The ups and downs of trophic control in continental shelf ecosystems. Trends Ecol. Evol. 22, 236–242. https://doi.org/10.1016/j.tree.2007.03.002

949 Garcia-Herrera, N., Cornils, A., Laudien, J., Niehoff, B., Höfer, J., Försterra, G.,
950 González, H.E., Richter, C., 2022. Seasonal and diel variations in the vertical
951 distribution, composition, abundance and biomass of zooplankton in a deep Chilean
952 Patagonian Fjord. PeerJ 10, e12823. https://doi.org/10.7717/peerj.12823

953 Garijo, J.C., Hernández-León, S., 2015. The use of an image-based approach for the
954 assessment of zooplankton physiological rates: a comparison with enzymatic methods.
955 J. Plankton Res. 37, 923–938. https://doi.org/10.1093/plankt/fbv056

956 Giering, S.L.C., Wells, S.R., Mayers, K.M.J., Schuster, H., Cornwell, L., Fileman, E.S.,
957 Atkinson, A., Cook, K.B., Preece, C., Mayor, D.J., 2019. Seasonal variation of
958 zooplankton community structure and trophic position in the Celtic Sea: A stable
959 isotope and biovolume spectrum approach. Prog. Oceanogr., Shelf Sea
960 Biogeochemistry: Pelagic Processes. 177, 101943.
961 https://doi.org/10.1016/j.pocean.2018.03.012

962 Gohin, F., 2011. Annual cycles of chlorophyll-*a*, non-algal suspended particulate
963 matter, and turbidity observed from space and in-situ in coastal waters. Ocean Sci. 7,
964 705–732. https://doi.org/10.5194/os-7-705-2011

965 González-Gil, R., Taboada, F.G., Höfer, J., Anadón, R., 2015. Winter mixing and
966 coastal upwelling drive long-term changes in zooplankton in the Bay of Biscay (1993–
967 2010). J. Plankton Res. 37, 337–351. https://doi.org/10.1093/plankt/fbv001

968 Gorsky, G., Ohman, M.D., Picheral, M., Gasparini, S., Stemmann, L., Romagnan, J.-
969 B., Cawood, A., Pesant, S., García-Comas, C., Prejger, F., 2010. Digital zooplankton
970 image analysis using the ZooScan integrated system. J. Plankton Res. 32, 285–303.
971 https://doi.org/10.1093/plankt/fbp124

972 Guillaud, J.-F., Aminot, A., Delmas, D., Gohin, F., Lunven, M., Labry, C., Herbland, A.,
973 2008. Seasonal variation of riverine nutrient inputs in the northern Bay of Biscay
974 (France), and patterns of marine phytoplankton response. J. Mar. Syst., Oceanography
975 of the Bay of Biscay 72, 309–319. https://doi.org/10.1016/j.jmarsys.2007.03.010

976 Hays, G., Richardson, A., Robinson, C., 2005. Climate change and marine plankton.
977 Trends Ecol. Evol. 20, 337–344. https://doi.org/10.1016/j.tree.2005.03.004

978 Hernández-León, S., Koppelmann, R., Fraile-Nuez, E., Bode, A., Mompeán, C.,
979 Irigoien, X., Olivar, M.P., Echevarría, F., Fernández de Puelles, M.L., González-

Gordillo, J.I., Cózar, A., Acuña, J.L., Agustí, S., Duarte, C.M., 2020. Large deep-sea zooplankton biomass mirrors primary production in the global ocean. Nat. Commun. 11, 6048. https://doi.org/10.1038/s41467-020-19875-7

Huret, M., Bourriau, P., Doray, M., Gohin, F., Petitgas, P., 2018. Survey timing vs. ecosystem scheduling: Degree-days to underpin observed interannual variability in marine ecosystems. Prog. Oceanogr. 166, 30–40. https://doi.org/10.1016/j.pocean.2017.07.007

Huret, M., Sourisseau, M., Petitgas, P., Struski, C., Léger, F., Lazure, P., 2013. A multi-decadal hindcast of a physical–biogeochemical model and derived oceanographic indices in the Bay of Biscay. J. Mar. Syst. 109–110, S77–S94. https://doi.org/10.1016/j.jmarsys.2012.02.009

ICES, 2010. Life-cycle spatial patterns of small pelagic fish in the Northeast Atlantic. ICES Coop. Res. Rep. 98.

Iriarte, A., Villate, F., Uriarte, I., Bidegain, G., Barroeta, Z., 2022. Shifts in neritic copepod communities off the Basque coast (southeastern Bay of Biscay) between 1998 and 2015. ICES J. Mar. Sci. 79, 830–843. https://doi.org/10.1093/icesjms/fsab265

Irigoien, X., Chust, G., Antonio Fernandes, J., Albaina, A., Zarauz, L., 2011. Factors determining the distribution and betadiversity of mesozooplankton species in shelf and coastal waters of the Bay of Biscay. J. Plankton Res. 33, 1182–1192. https://doi.org/10.1093/plankt/fbr026

Irigoien, X., Fernandes, J.A., Grosjean, P., Denis, K., Albaina, A., Santos, M., 2008. Spring zooplankton distribution in the Bay of Biscay from 1998 to 2006 in relation with anchovy recruitment. J. Plankton Res. 31, 1–17. https://doi.org/10.1093/plankt/fbn096

Josse, J., Husson, F., 2016. missMDA : A Package for Handling Missing Values in Multivariate Data Analysis. J. Stat. Softw. 70. https://doi.org/10.18637/jss.v070.i01

Kerkar, A.U., Venkataramana, V., Tripathy, S.C., 2022. Assessing the trophic link between primary and secondary producers in the Southern Ocean: A carbon-biomass based approach. Polar Sci. 31, 100734. https://doi.org/10.1016/j.polar.2021.100734

1009 Koutsikopoulos, C., Beillois, P., Leroy, C., Taillefer, F., 1998. Temporal trends and
1010 spatial structures of the sea surface temperature in the Bay of Biscay. Oceanol. Acta
1011 21, 335–344. https://doi.org/10.1016/S0399-1784(98)80020-0

1012 Koutsikopoulos, C., Le Cann, B., 1996. Physical processes and hydrological structures
1013 related to the Bay of Biscay anchovy. Sci. Mar. 9–19.

1014 Kupschus, S., Schratzberger, M., Righton, D., 2016. Practical implementation of
1015 ecosystem monitoring for the ecosystem approach to management. J. Appl. Ecol. 53,
1016 1236–1247. https://doi.org/10.1111/1365-2664.12648

1017 Lê, S., Josse, J., Husson, F., 2008. FactoMineR: An R Package for Multivariate
1018 Analysis. J. Stat. Softw. 25, 1–18. https://doi.org/10.18637/jss.v025.i01

1019 Lehette, P., Hernández-León, S., 2009. Zooplankton biomass estimation from digitized
1020 images: a comparison between subtropical and Antarctic organisms: Zooplankton
1021 biomass by digital images. Limnol. Oceanogr. Methods 7, 304–308.
1022 https://doi.org/10.4319/lom.2009.7.304

1023 Makhlouf Belkahia, N., Pagano, M., Chevalier, C., Devenon, J.L., Daly Yahia, M.N.,
1024 2021. Zooplankton abundance and community structure driven by tidal currents in a
1025 Mediterranean coastal lagoon (Boughrara, Tunisia, SW Mediterranean Sea). Estuar.
1026 Coast. Shelf Sci. 250, 107101. https://doi.org/10.1016/j.ecss.2020.107101

1027 Marcolin, C. da R., Schultes, S., Jackson, G.A., Lopes, R.M., 2013. Plankton and
1028 seston size spectra estimated by the LOPC and ZooScan in the Abrolhos Bank
1029 ecosystem (SE Atlantic). Cont. Shelf Res. 70, 74–87.
1030 https://doi.org/10.1016/j.csr.2013.09.022

1031 Marcolin, C.R., Gaeta, S., Lopes, R.M., 2015. Seasonal and interannual variability of
1032 zooplankton vertical distribution and biomass size spectra off Ubatuba, Brazil. J.
1033 Plankton Res. 37, 808–819. https://doi.org/10.1093/plankt/fbv035

1034 Masse, J., Uriarte, A., Angelico, M., Carrera, P., 2018. Pelagic survey series for sardine
1035 and anchovy in ICES subareas 8 and 9 — Towards an ecosystem approach. ICES
1036 Coop. Res. Rep. https://doi.org/10.17895/ices.pub.4599

1037 Mitra, A., Davis, C., 2010. Defining the “to” in end-to-end models. Prog. Oceanogr.,
1038 Special Issue: Parameterisation of Trophic Interactions in Ecosystem Modelling 84,
1039 39–42. https://doi.org/10.1016/j.pocean.2009.09.004

1040 Morse, R.E., Friedland, K.D., Tommasi, D., Stock, C., Nye, J., 2017. Distinct
1041 zooplankton regime shift patterns across ecoregions of the U.S. Northeast continental
1042 shelf Large Marine Ecosystem. J. Mar. Syst. 165, 77–91.
1043 https://doi.org/10.1016/j.jmarsys.2016.09.011

1044 Noyon, M., Poulton, A.J., Asdar, S., Weitz, R., Giering, S.L.C., 2022. Mesozooplankton
1045 community distribution on the Agulhas Bank in autumn: Size structure and production
1046 | Elsevier Enhanced Reader. Deep-Sea Part II 195.
1047 https://doi.org/10.1016/j.dsr2.2021.105015

1048 Pagès, J., 2014. Multiple Factor Analysis by Example Using R, 1st ed. Chapman and
1049 Hall/CRC. https://doi.org/10.1201/b17700

1050 Pepin, P., Johnson, C.L., Harvey, M., Casault, B., Chassé, J., Colbourne, E.B.,
1051 Galbraith, P.S., Hebert, D., Lazin, G., Maillet, G., Plourde, S., Starr, M., 2015. A
1052 multivariate evaluation of environmental effects on zooplankton community structure
1053 in the western North Atlantic. Prog. Oceanogr. 134, 197–220.
1054 https://doi.org/10.1016/j.pocean.2015.01.017

1055 Petitgas, P., Doray, M., Huret, M., Massé, J., Woillez, M., 2014. Modelling the variability
1056 in fish spatial distributions over time with empirical orthogonal functions: anchovy in
1057 the Bay of Biscay. ICES J. Mar. Sci. 71, 2379–2389.
1058 https://doi.org/10.1093/icesjms/fsu111

1059 Petitgas, P., Goarant, A., Massé, J., Bourriau, P., 2009. Combining acoustic and
1060 CUFES data for the quality control of fish-stock survey estimates. ICES J. Mar. Sci.
1061 66, 1384–1390. https://doi.org/10.1093/icesjms/fsp007

1062 Petitgas, P., Huret, M., Dupuy, C., Spitz, J., Authier, M., Romagnan, J.B., Doray, M.,
1063 2018. Ecosystem spatial structure revealed by integrated survey data. Prog.
1064 Oceanogr., Multidisciplinary integrated surveys 166, 189–198.
1065 https://doi.org/10.1016/j.pocean.2017.09.012

1066 Picheral, M., Colin, S., Irisson, J.O., 2017. EcoTaxa, a tool for the taxonomic
1067 classification of images. URL Httpecotaxa Obs-Vlfr Fr.

1068 Planque, B., Lazure, P., Jégou, A.-M., 2004. Detecting hydrological landscapes over
1069 the Bay of Biscay continental shelf in spring. Clim. Res. 28, 41–52.
1070 https://doi.org/10.3354/cr028041

1071 Plounevez, S., Champalbert, G., 1999. Feeding Behaviour and Trophic Environment
1072 of Engraulis encrasicolus (L.) in the Bay of Biscay. Estuar. Coast. Shelf Sci. 49, 177–
1073 191. https://doi.org/10.1006/ecss.1999.0497

1074 Queiros, Q., Fromentin, J.-M., Gasset, E., Dutto, G., Huiban, C., Metral, L., Leclerc, L.,
1075 Schull, Q., McKenzie, D.J., Saraux, C., 2019. Food in the Sea: Size Also Matters for
1076 Pelagic Fish. Front. Mar. Sci. 6.

1077 Romagnan, J.B., Aldamman, L., Gasparini, S., Nival, P., Aubert, A., Jamet, J.L.,
1078 Stemmann, L., 2016. High frequency mesozooplankton monitoring: Can imaging
1079 systems and automated sample analysis help us describe and interpret changes in
1080 zooplankton community composition and size structure - An example from a coastal
1081 site. J. Mar. Syst. 162, 18–28. https://doi.org/10.1016/j.jmarsys.2016.03.013

1082 Romagnan, J.-B., Legendre, L., Guidi, L., Jamet, J.-L., Jamet, D., Mousseau, L.,
1083 Pedrotti, M.-L., Picheral, M., Gorsky, G., Sardet, C., Stemmann, L., 2015.
1084 Comprehensive Model of Annual Plankton Succession Based on the Whole-Plankton
1085 Time Series Approach. PLOS ONE 10, e0119219.
1086 https://doi.org/10.1371/journal.pone.0119219

1087 Rykaczewski, R.R., Checkley, D.M., 2008. Influence of ocean winds on the pelagic
1088 ecosystem in upwelling regions. Proc. Natl. Acad. Sci. 105, 1965–1970.
1089 https://doi.org/10.1073/pnas.0711777105

1090 Saraux, C., Van Beveren, E., Brosset, P., Queiros, Q., Bourdeix, J.-H., Dutto, G.,
1091 Gasset, E., Jac, C., Bonhommeau, S., Fromentin, J.-M., 2019. Small pelagic fish
1092 dynamics: A review of mechanisms in the Gulf of Lions. Deep Sea Res. Part II Top.
1093 Stud. Oceanogr., Drivers of dynamics of small pelagic fish resources: environmental
1094 control of long-term changes 159, 52–61. https://doi.org/10.1016/j.dsr2.2018.02.010

1095 Saulquin, B., Gohin, F., 2010. Mean seasonal cycle and evolution of the sea surface
1096 temperature from satellite and in situ data in the English Channel for the period 1986–
1097 2006. Int. J. Remote Sens. 31, 4069–4093.
1098 https://doi.org/10.1080/01431160903199155

Sourisseau, M., Carlotti, F., 2006. Spatial distribution of zooplankton size spectra on the French continental shelf of the Bay of Biscay during spring 2000 and 2001. J. Geophys. Res. Oceans 111. https://doi.org/10.1029/2005JC003063

Soviadan, Y.D., Benedetti, F., Brandão, M.C., Ayata, S.-D., Irisson, J.-O., Jamet, J.L., Kiko, R., Lombard, F., Gnandi, K., Stemmann, L., 2022. Patterns of mesozooplankton community composition and vertical fluxes in the global ocean. Prog. Oceanogr. 200, 102717. https://doi.org/10.1016/j.pocean.2021.102717

Stige, L.C., Dalpadado, P., Orlova, E., Boulay, A.-C., Durant, J.M., Ottersen, G., Stenseth, N.Chr., 2014. Spatiotemporal statistical analyses reveal predator-driven zooplankton fluctuations in the Barents Sea. Prog. Oceanogr. 120, 243–253. https://doi.org/10.1016/j.pocean.2013.09.006

Stirnimann, L., Bornman, T.G., Verheye, H.M., Bachèlery, M.-L., van der Poel, J., Fawcett, S.E., 2021. Plankton community composition and productivity near the Subantarctic Prince Edward Islands archipelago in autumn. Limnol. Oceanogr. 66, 4140–4158. https://doi.org/10.1002/lno.11949

Valdes, L., Lopez-Urrutia, A., Beaugrand, G., Harris, R.P., Irigoien, X., 2022. Seasonality and interannual variability of copepods in the Western English Channel, Celtic Sea, Bay of Biscay, and Cantabrian Sea with a special emphasis to *Calanus helgolandicus* and *Acartia clausi*. ICES J. Mar. Sci. 79, 727–740. https://doi.org/10.1093/icesjms/fsac052

Van Der Lingen, C.D., 2002. Diet of sardine Sardinops sagax in the southern Benguela upwelling ecosystem. South Afr. J. Mar. Sci. 24, 301–316. https://doi.org/10.2989/025776102784528691

Vandromme, P., Nogueira, E., Huret, M., Lopez-Urrutia, Á., González-Nuevo González, G., Sourisseau, M., Petitgas, P., 2014. Springtime zooplankton size structure over the continental shelf of the Bay of Biscay. Ocean Sci. 10, 821–835. https://doi.org/10.5194/os-10-821-2014

Vandromme, P., Stemmann, L., Garcìa-Comas, C., Berline, L., Sun, X., Gorsky, G., 2012. Assessing biases in computing size spectra of automatically classified zooplankton from imaging systems: A case study with the ZooScan integrated system. Methods Oceanogr. 1–2, 3–21. https://doi.org/10.1016/j.mio.2012.06.001

Zarauz, L., Irigoien, X., Fernandes, J.A., 2008. Modelling the influence of abiotic and biotic factors on plankton distribution in the Bay of Biscay, during three consecutive years (2004-06). J. Plankton Res. 30, 857–872. https://doi.org/10.1093/plankt/fbn049

Zarauz, L., Irigoien, X., Urtizberea, A., Gonzalez, M., 2007. Mapping plankton distribution in the Bay of Biscay during three consecutive spring surveys. Mar. Ecol. Prog. Ser. 345, 27–39. https://doi.org/10.3354/meps06970

# 9 Supplementary Materials

## A. Missing data imputation

Following the spatial gridding procedure, some data were missing, due to missing sampling stations in the northern part of the Bay, mostly at the beginning of the time series (Table A.1). Following Josse & Husson (2016), an algorithm based on iterative Principal Components Analysis (PCA) from the MissMDA *R* library was used to impute estimated values in lace of the missing ones in the hydrology, phytoplankton and mesozooplankton datasets. For each variable, the data were organized in matrix grid cells x years. The first step of the algorithm consisted in the imputation of missing values with the annual means (for example, if the grid cell numbered 33 had not Acartiidae's biomass in 2004, it was filled with the 2004 mean Acartiidae's biomass). Then, a first PCA was performed on the imputed matrix and the estimated values replaced the annual mean values previously imputed to fill the missing data. Then, a second PCA was performed and the estimated values from the first PCA were replaced by the estimated value from the second PCA. The algorithm kept running iteratively until the difference between two successive estimated values was smaller than a threshold (set at 1e-06 by default ; Josse & Husson, 2016).

Table A1: Number and percentage of grid cells with missing data each year.

| Years | Number of missing cells | Percentage of missing cells |
|---|---|---|
| 2004 | 6 | 5 |
| 2005 | 17 | 14.1 |
| 2006 | 22 | 18.2 |
| 2007 | 12 | 9.9 |
| 2008 | 4 | 3.3 |
| 2009 | 0 | 0 |
| 2010 | 0 | 0 |
| 2011 | 2 | 1.7 |
| 2012 | 5 | 4 |
| 2013 | 5 | 4 |
| 2014 | 2 | 1.7 |
| 2015 | 0 | 0 |
| 2016 | 0 | 0 |
| 2017 | 0 | 0 |
| 2018 | 0 | 0 |
| 2019 | 1 | 0.8 |

## B. Annual spatial clustering

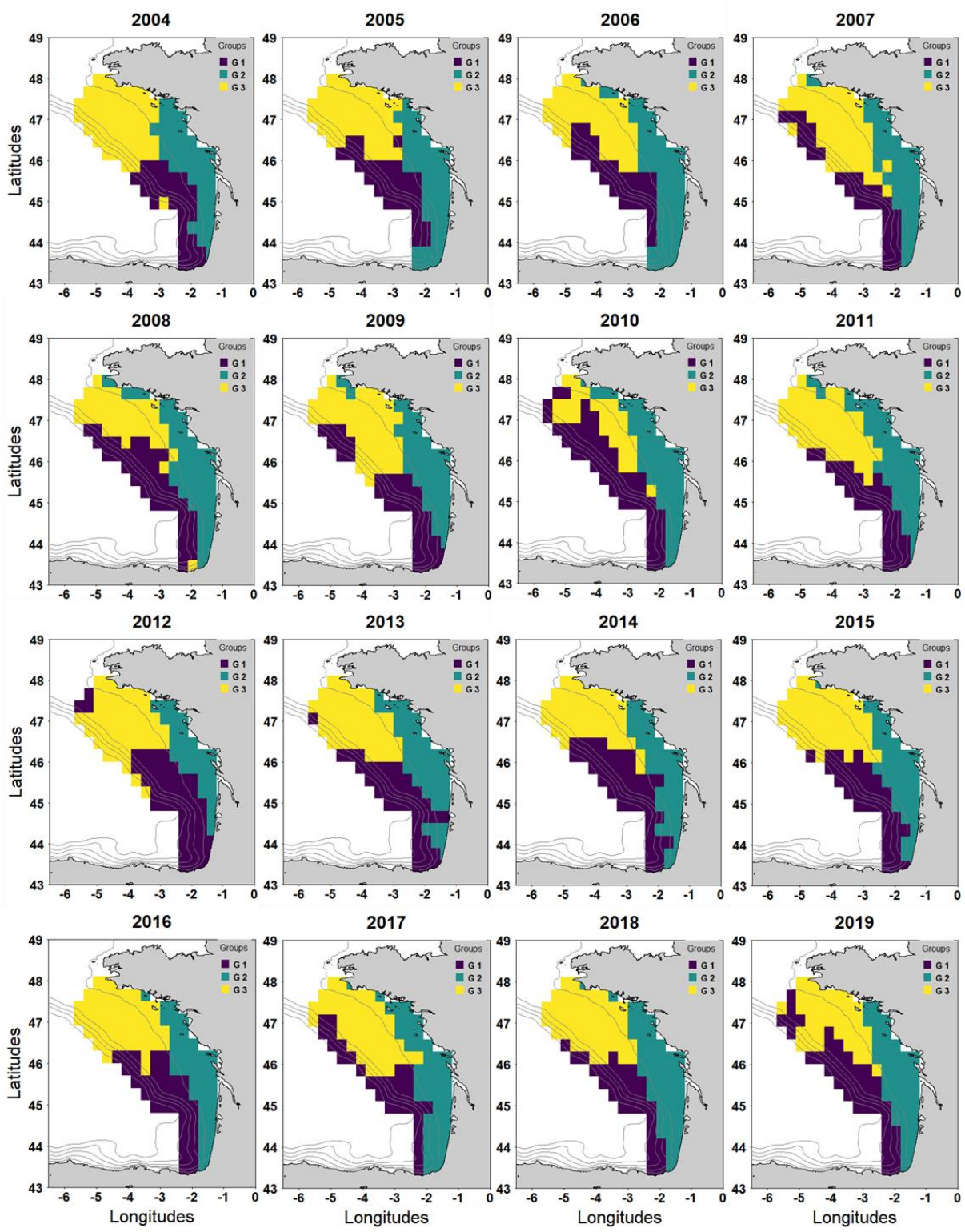


Fig. B1: Annual spatial extent of the clusters identified with the hierarchical clustering of grid cells in the mesozooplankton Multi Factor Analysis factorial space.

## C. Correlates of the observed mesozooplankton space-time patterns

Table C.1: Variance Inflation Factor (VIF) calculated for each Multi Factor Analysis selected principal component in the hydrology, primary producers and small pelagic fish datasets, which are used as predictors in Generalized Linear Models. A VIF value higher than five identifies problematic multicollinearity among predictors.

| Principal components | hydroMFA1 | hydroMFA2 | hydroMFA3 | phytoMFA1 | spfMFA1 | spfMFA2 |
|---|---|---|---|---|---|---|
| VIF values | 12.6 | 13.9 | 3.7 | 12.3 | 7.4 | 10.1 |

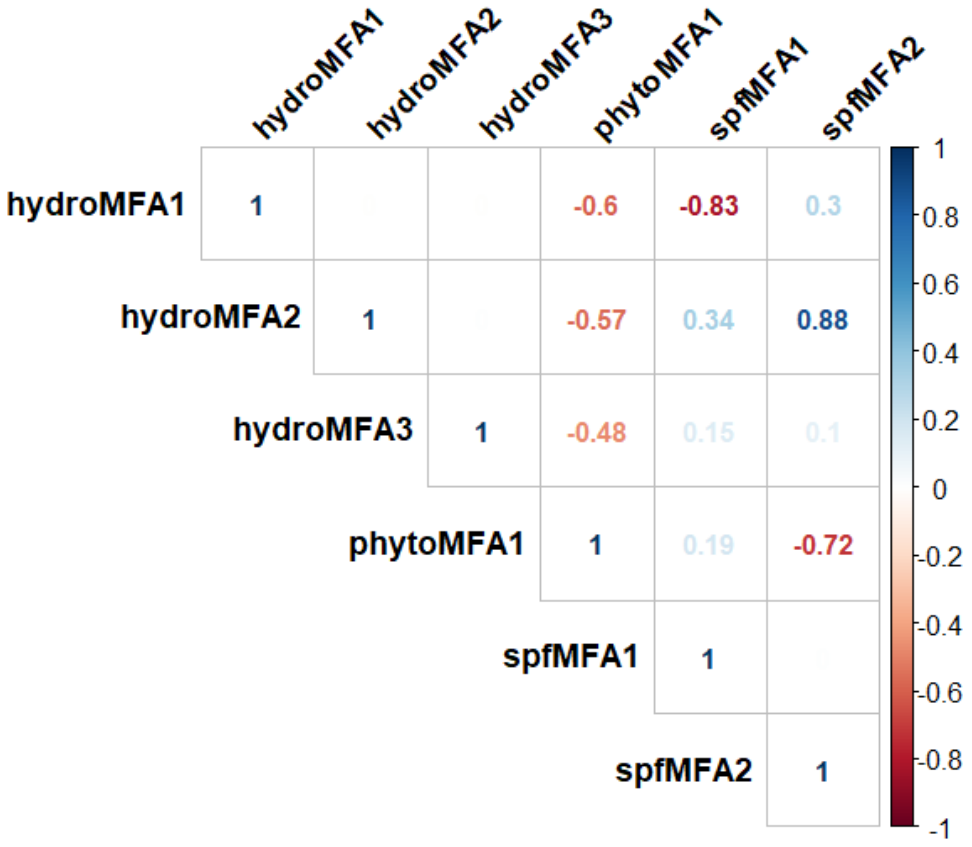


Fig. C.1: Correlation coefficients among all the predictors.

Table C.2: Results of the stepwise backward model selection procedure showing the models explaining the first principal component in the mesozooplankton Multi Factor Analysis zooMFA1 and their Akaïke's Information Criterion (AIC).

| Predictors included in the model | AIC |
|---|---|
| hydroMFA1 + hydroMFA2 + hydroMFA3 + spfMFA1 | 450.05 |
| hydroMFA1 + hydroMFA2 + spfMFA1 | 451.31 |
| hydroMFA1 + hydroMFA3 + spfMFA1 | 473.49 |
| hydroMFA1 + hydroMFA2 + hydroMFA3 | 479.17 |
| hydroMFA2 + hydroMFA3 + spfMFA1 | 491.39 |

Table C.3 Results of the stepwise backward model selection procedure showing the models explaining the second principal component in the mesozooplankton Multi Factor Analysis zooMFA2 and their Akaïke's Information Criterion (AIC).

| Predictors included in the model | AIC |
|---|---|
| hydroMFA2 + hydroMFA3 + spfMFA1 | 311.93 |
| hydroMFA2 + spfMFA1 | 310.57 |
| hydroMFA2 | 310.73 |
| spfMFA1 | 771.64 |